Research paper

Identification of the first-in-class dual inhibitor targeting BAG3 and HSP70 proteins to disrupt multiple chaperone pathways

Dafne Ruggiero [a,1], Emis Ingenito [b,1], Eleonora Boccia [a], Vincenzo Vestuto [a], Gilda D'Urso [a], Alessandra Capuano [a], Agostino Casapullo [a], Stefania Terracciano [a], Giuseppe Bifulco [a], Gianluigi Lauro [a,**], Ines Bruno [a,*]

[a] *Department of Pharmacy, University of Salerno, Via Giovanni Paolo II 132, 84084, Fisciano, Italy*
[b] *Institute of Molecular and Translational Medicine, Faculty of Medicine and Dentistry and Czech Advanced Technology and Research Institute, Palacky University in Olomouc, Křížkovského 511/8, 779 00, Olomouc, Czech Republic*

A B S T R A C T

In the complex network of cellular physiology, the maintenance of cellular proteostasis emerges as a critical factor for cell survival, particularly under stress conditions. This homeostasis is largely governed by a sophisticated network of molecular chaperones and co-chaperones, among which Bcl-2-associated athanogene 3 (BAG3), able to interact with the ATPase domain of Heat Shock Protein 70 (HSP70), plays a pivotal role. The BAG3-HSP70 functional module is not only essential for cellular homeostasis but is also involved in the pathogenesis of various diseases, including cancer, neurodegenerative disorders, and cardiac dysfunction, making it an attractive target for therapeutic intervention. Inspired by our continuous interest in the development of new chemical platforms able to interfere with BAG3 protein, herein we report the discovery of compound **16**, the first-in-class BAG3/HSP70 dual modulator, obtained by combining the multicomponent Ugi reaction with the alkyne-azide Huisgen procedure in a sequential tandem reaction approach. Through a combination of biophysical analysis, biochemical assays, and cell-based studies, we elucidated the mechanism of action of this inhibitor and assessed its potential as a therapeutic agent. Hence, this study can open new avenues for the development of novel anticancer strategies that leverage the simultaneous disruption of multiple chaperone pathways.

1. Introduction

Cancer cells exploit the protein quality control system to manage the stress associated with rapid proliferation and environmental toxic conditions [1–4]. Within this system, the co-chaperone BAG3, which interacts with HSP70 through its conserved BAG domain forming a functional module, is of particular interest due to its role in supporting cancer cell survival, suppressing apoptosis, and facilitating the autophagic removal of damaged proteins [5,6]. Besides BAG3 own independent functions, the BAG3/HSP70 axis is implicated in the pathogenesis of various cancers, making it an attractive target for drug development. Recent advancements in the understanding of BAG3 and HSP70 mechanisms have highlighted their synergistic action in

facilitating tumor growth, metastasis, and resistance to chemotherapy [7–11]. The individual inhibition of BAG3 and HSP70 has been explored during the last years as a therapeutic strategy against cancer; however, the absence of a co-crystallized structure of human BAG3-inhibitor coupled with the structural complexity of HSP70, undergoing conformational changes during its chaperone cycle, has posed significant challenges for computer-aided structure-based approaches in the discovery of modulators. From a structural point of view, BAG3, belonging to the BAG family of co-chaperones, is a 575 amino acids protein showing a multimodular architecture; indeed, besides the BAG domain, BAG3 includes also four well-defined binding sites: a WW domain, a PXXP region and two IPV motifs which contribute to a large interactome and participation in a wide range of cellular functions [12–17]. Most of

its cytoprotective and prosurvival functions are ascribed to the modulation of the ATP-dependent HSP70 chaperone and as a fact, the two proteins are found to be co-elevated in several cancer types and are associated with resistance to chemotherapy [18–23]. However, despite the intricate biology of BAG3 protein being progressively unveiled, the medicinal chemistry efforts did not achieve the desired success.

In 2018, our research group made a significant breakthrough by identifying the first modulator of BAG3, **LK4**, which features a thiazolidinedione core [24]. This discovery represented a critical advancement in the exploration of BAG3 as a therapeutic target, particularly in the context of cancer treatment. Building upon this initial finding, we conducted further investigations, introducing subtle structural modifications to **LK4**, which culminated in the development of a second, more potent and selective BAG3 inhibitor in 2022 [25]. Subsequently, in 2023, the research conducted by Budassi's group extended this work by introducing more extensive structural modifications to **LK4**, resulting in the identification of a new BAG3 modulator with significant effects on autophagy and the stabilization of client proteins [26]. Finally, in 2024, our team made another noteworthy advancement by identifying a novel BAG3 modulator with a completely distinct scaffold—imidazopyridine—thereby marking a significant progression in the pursuit of alternative and potentially more effective approaches to targeting BAG3 in therapeutic applications [27]. Notably, allosteric inhibitors of the BAG3-HSP70 interaction, such as **YM-01** and **JG-98**, have been widely used in research and therapeutic contexts. **YM-01** is a selective inhibitor of HSP70 ATPase activity and is commonly utilized in preclinical studies to investigate HSP70's role in various cellular processes. Its use as a positive control in BAG3 studies has been valuable due to its targeted effects on HSP70 with minimal off-target interference [28]. Conversely, **JG-98** is a more potent inhibitor of HSP70, designed primarily for therapeutic applications. It has shown effectiveness in disrupting HSP70's role in cancer cells [29]. However, if compared to **YM-01**, **JG-98** demonstrates stronger HSP70 inhibition, but its broader impact on multiprotein interactions may complicate its use in studies specifically focused on the BAG3-HSP70 axis. These advancements highlight the scientific potential and therapeutic implications of targeting the BAG3-HSP70 complex, emphasizing its importance in cancer treatment and diseases driven by cellular stress and imbalances in proteostasis.

Prompted by our constant interest in the development of new chemical platforms able to interfere with BAG3 protein, we decided to exploit the modular nature of the multicomponent reactions, combining in a sequential tandem approach the Ugi reaction with the alkyne-azide Huisgen procedure to obtain a new class of 1,2,3-triazole-α-acylaminocarboxamides which were submitted to physiochemical and biological evaluation [30,31]. These findings enabled us to disclose compound **16** which, to our knowledge, represents the first chemical agent able to simultaneously interfere with both BAG3 and HSP70 proteins. It emerged as a promising new drug prototype that could offer a novel therapeutic approach with enhanced efficacy against cancer, and it could certainly contribute to provide valuable insights into the feasibility of targeting the BAG3/HSP70 axis.

2. Results and discussion

2.1. Synthesis

To interrogate the target of interest and identify new attractive binders, we planned to use molecular probes featuring the triazole scaffold due to the multiple opportunities it offers as a privileged structure. Since combination of click chemistry with multicomponent reactions (MCRs) represents a powerful strategy in organic synthesis to enhance structural diversity, we decided to employ a tandem reaction approach, utilizing the Ugi four-component procedure followed by the CuAAC (copper-catalyzed azide-alkyne cycloaddition) reaction [32,33]. In detail, the one-pot condensation of aldehydes (**a**, **b**), isocyanides (**c**,

d), amines (**e-i**), and α-chloroacetic acid yielded Ugi-type chlorides (**I**), which were then converted into the corresponding azides (**II**) after treatment with sodium azide and potassium carbonate in DMA at room temperature. The resulting Ugi-azides were subjected to a CuAAC reaction with selected alkynes (**j-l**). The reaction, carried out in a mixture of t-BuOH, H_2O, and DMSO (4:2:1), in the presence of copper sulfate and sodium ascorbate at room temperature, afforded the final products in high yield [34]. The 1,2,3-triazoles (**1-10**) were easily isolated through aqueous workup and characterized using spectroscopic methods (Fig. 1).

2.2. Biophysical assays

To evaluate the affinity of the synthesized molecules (**1-10**) for the protein counterpart, Surface Plasmon Resonance (SPR) assays were performed against full-length BAG3 and its isolated BAG domain (BD). Protein immobilization was achieved using the amide coupling method, and the molecules were tested at 10 different concentrations, ranging from 0 to 100 μM. A known BAG3-BD binder, **LK4** ((Z)-ethyl 2-(5-(3,4-dihydroxybenzylidene)-2,4-dioxothiazolidin-3-yl)acetate), was used as a positive control [24,28]. Among the 10 molecules tested, only compound **7** exhibited satisfactory affinity for both full-length BAG3 (K_D = 64.00 ± 2.25 μM) and its BAG domain (K_D = 32.50 ± 2.47 μM) (Table 1).

2.3. Viability assays

Elevated BAG3 expression is closely linked to signaling pathways in various malignant cell types, hence, the activity reduction of this chaperone inhibits cell proliferation, triggers apoptosis, and induces cell cycle arrest [8,10]. To assess the activity of compound **7**, cytotoxicity assays were performed on a small panel of cell lines known for over-expressing BAG3. MTT assays were conducted on A549 (lung adenocarcinoma), HeLa (cervical carcinoma), and A375 (malignant melanoma) cells, exposing them to different concentrations of compound **7** (10 and 50 μM) for 72 h [25,35–37]. Additionally, 10 % DMSO was used as a positive control and 0.1 % DMSO as a negative control. Moreover, together with the negative and positive controls with DMSO, the known IC_{50} values of **LK4** on the cell lines tested after 72 h of treatment were also considered: A549: 32.3 ± 0.9 μM; HeLa: >50 μM; A375: 16.6 ± 1.5 μM [28]. Unfortunately, compound **7** exhibited significant cytotoxic activity only at high concentrations on A549 and HeLa cells (Fig. 2).

2.4. Computational studies

Once established the viability of the Ugi-Huisgen type framework for target exploration, we decided to expand our compounds collection, aiming at enhancing the biological profile of our disclosed hit **7**. To this purpose, a computer-aided approach (Fig. 3) was carried out to gain useful insights for the hit optimization process.

The binding of this set of compounds with the protein was predicted through molecular docking calculations to obtain a reference binding mode and to identify the fundamental amino acids of the binding site for aiding the selection of further promising compounds. The result highlighted that compound **7** is placed onto the binding site by interacting with Ser6, through a halogen bond, with Lys93, through π-cation interactions with the triazole moiety, and with Arg92, through H-bonds. Starting from the results obtained for this compound, a combinatorial library was built considering the privileged scaffold and the possibility of decorating it according to the commercial availability of the related synthons. The 1,2,3-triazole derivatives were obtained by modifying the alkynes (at the R4 position) and the aromatic aldehydes (at the R1 position). Accordingly, starting from commercially available items, a combinatorial virtual library of ~17,000 compounds was built and used as input for molecular docking calculations against the murine BAG-binding domain of BAG3 (BAG3-BD, *see Computational Details*) (Figs. 3
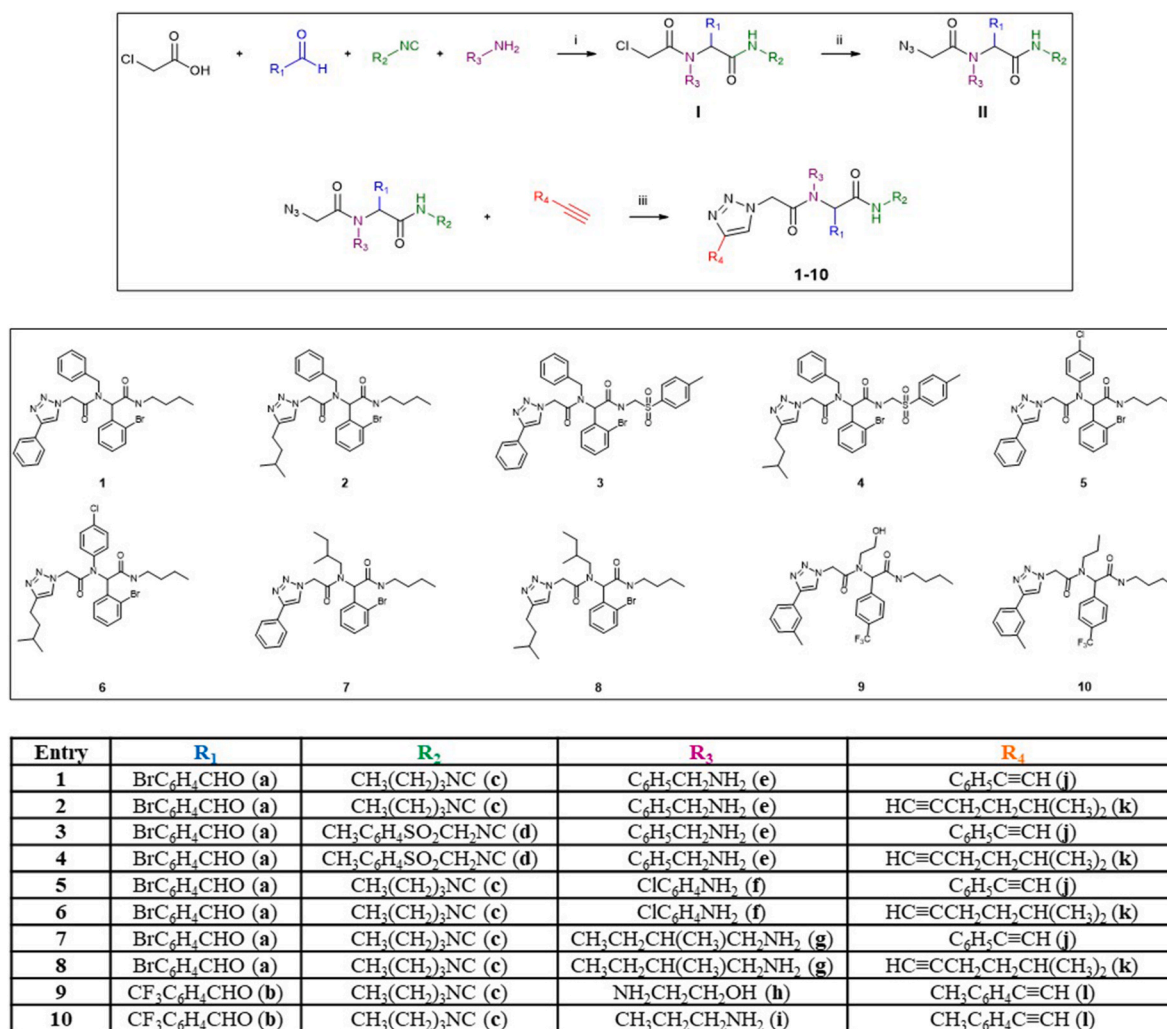
Fig. 1. Structures and synthesis of compounds **1–10** by Ugi-Huisgen reaction. Reagents and conditions: (**i**) CH₂Cl₂, rt, 48–72 h (63–89 %); (**ii**) NaN₃, K₂CO₃, DMA, rt, 4 h; (**iii**) CuSO₄·5H₂O, sod. ascorbate, DMSO/t-BuOH/H₂O, rt, 12 h (32–96 %).

Entry	R₁	R₂	R₃	R₄
1	BrC₆H₄CHO (a)	CH₃(CH₂)₃NC (c)	C₆H₅CH₂NH₂ (e)	C₆H₅C≡CH (j)
2	BrC₆H₄CHO (a)	CH₃(CH₂)₃NC (c)	C₆H₅CH₂NH₂ (e)	HC≡CCH₂CH₂CH(CH₃)₂ (k)
3	BrC₆H₄CHO (a)	CH₃C₆H₄SO₂CH₂NC (d)	C₆H₅CH₂NH₂ (e)	C₆H₅C≡CH (j)
4	BrC₆H₄CHO (a)	CH₃C₆H₄SO₂CH₂NC (d)	C₆H₅CH₂NH₂ (e)	HC≡CCH₂CH₂CH(CH₃)₂ (k)
5	BrC₆H₄CHO (a)	CH₃(CH₂)₃NC (c)	ClC₆H₄NH₂ (f)	C₆H₅C≡CH (j)
6	BrC₆H₄CHO (a)	CH₃(CH₂)₃NC (c)	ClC₆H₄NH₂ (f)	HC≡CCH₂CH₂CH(CH₃)₂ (k)
7	BrC₆H₄CHO (a)	CH₃(CH₂)₃NC (c)	CH₃CH₂CH(CH₃)CH₂NH₂ (g)	C₆H₅C≡CH (j)
8	BrC₆H₄CHO (a)	CH₃(CH₂)₃NC (c)	CH₃CH₂CH(CH₃)CH₂NH₂ (g)	HC≡CCH₂CH₂CH(CH₃)₂ (k)
9	CF₃C₆H₄CHO (b)	CH₃(CH₂)₃NC (c)	NH₂CH₂CH₂OH (h)	CH₃C₆H₄C≡CH (l)
10	CF₃C₆H₄CHO (b)	CH₃(CH₂)₃NC (c)	CH₃CH₂CH₂NH₂ (i)	CH₃C₆H₄C≡CH (l)

Table 1

SPR assays of compounds **1–10** and **LK4** on BAG3 full length and BAG3-BD. K_D = dissociation constant; SD = standard deviation.

Compound	BAG3 FULL K_D (µM) ± SD	BAG-BD K_D (µM) ± SD
1	No binding	Not determined
2	No binding	Not determined
3	No binding	Not determined
4	33.70 ± 1.65	No binding
5	26.20 ± 4.88	No binding
6	No binding	Not determined
7	64.00 ± 2.25	32.50 ± 2.47
8	No binding	Not determined
9	18.80 ± 6.01	No binding
10	Poor solubility	Poor solubility
LK4	19.90 ± 6.58	0.18 ± 0.02

and 4).

To reduce the number of compounds, the virtual library was screened against compound **7**, specifically computing the related shape similarity values (Phase software) and considering its predicted binding mode. In this manner, a subset of compounds was selected from the original library with a shape comparable to that of the disclosed hit compound **7**, saving those featured with a shape similarity value higher than 0.700 (this shape similarity value can vary from zero, with no
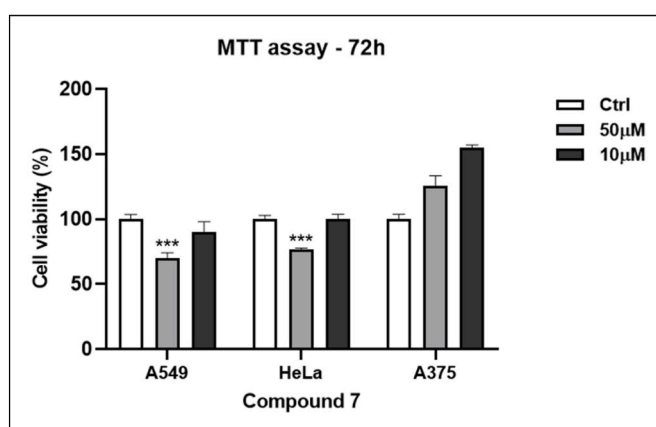

Fig. 2. The antiproliferative activity of compound **7** was evaluated on the human lung adenocarcinoma cell line (A549), the human cervical adenocarcinoma cell line (HeLa) and the human melanoma cell line (A375) after 72 h of treatment at concentrations of 10 µM and 50 µM. The positive control (CTRL POS) consisted of 10 % DMSO, while the negative control (CTRL NEG) consisted of 0.1 % DMSO. Results are showed as mean ± standard deviation (SD) from three independent experiments. *** denotes p < 0.001 vs. Ctrl.
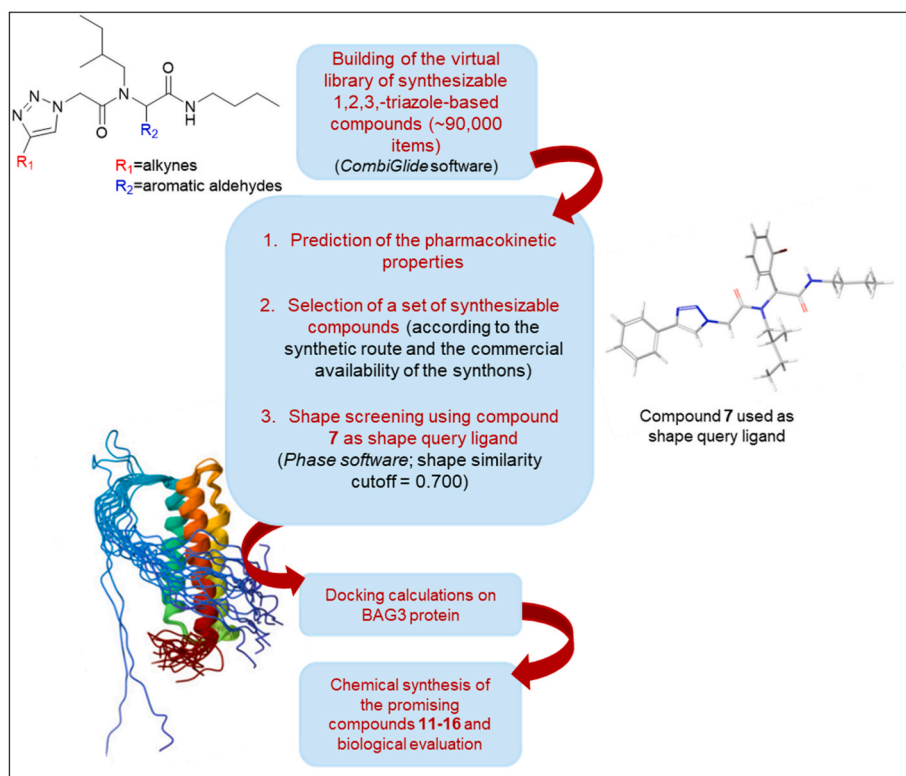
Fig. 3. Computational workflow leading to the selection of the promising compounds **11–16**.
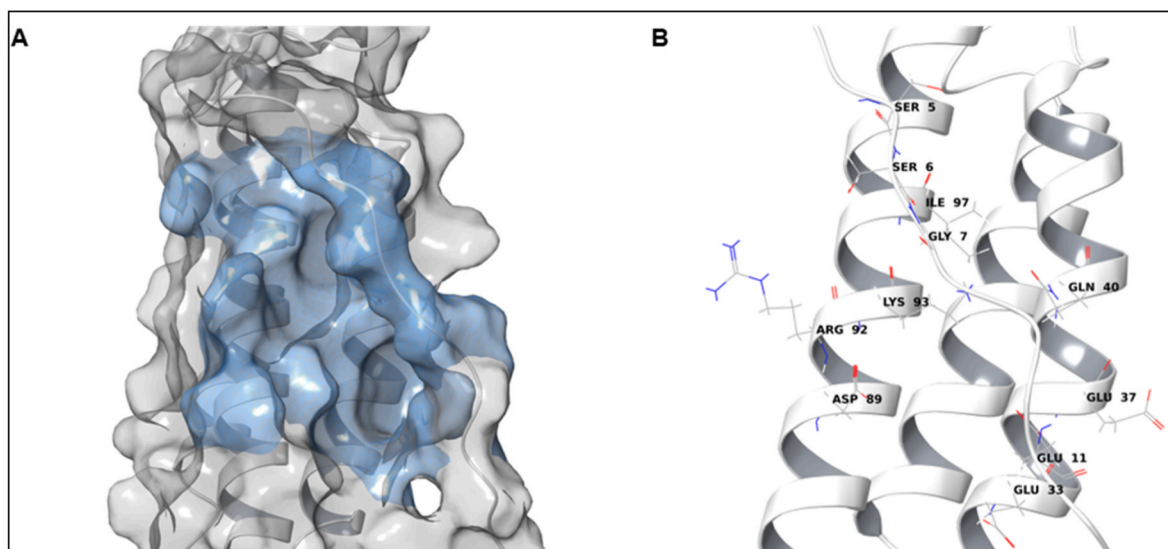

Fig. 4. (**a**) 3D structure of BAG3 (PDB: 1UK5, in blue the binding site). (**b**) Representation of the amino acids involved in the binding site. (For interpretation of the references to color in this figure legend, the reader is referred to the Web version of this article.)

matching atoms between the reference compound and those screened, to one, with all atoms matching). The subset of selected compounds was then used as input for the subsequent molecular docking calculations. The most promising compounds were then identified after a visual inspection step, filtering and synthesizing those able to interact with the fundamental amino acids of the BAG3 binding site and resembling a binding mode comparable to that of the hit compound **7** (**11–16**) (Fig. 5a). Indeed, the analysis of the binding mode of these promising compounds showed their ability to interact with the protein establishing contacts with the above-reported amino acids (i.e., Ser6, Arg92, and Lys93) (Fig. 5b and c).

2.5. Synthesis

The most promising selected compounds **11–16** were synthesized using the previously reported synthetic strategy, as outlined in Fig. 1. To obtain the Ugi-chlorides, a combination of seven aldehydes (**m-r**), one isocyanide (**c**), one amine (**g**), and α-chloroacetic acid was used. These intermediates were then treated with sodium azide to produce the corresponding azides. Finally, the azides underwent a Huisgen cycloaddition reaction with seven alkynes (**t-x**), yielding final products **11–16** in high yields, as shown in Fig. 6.
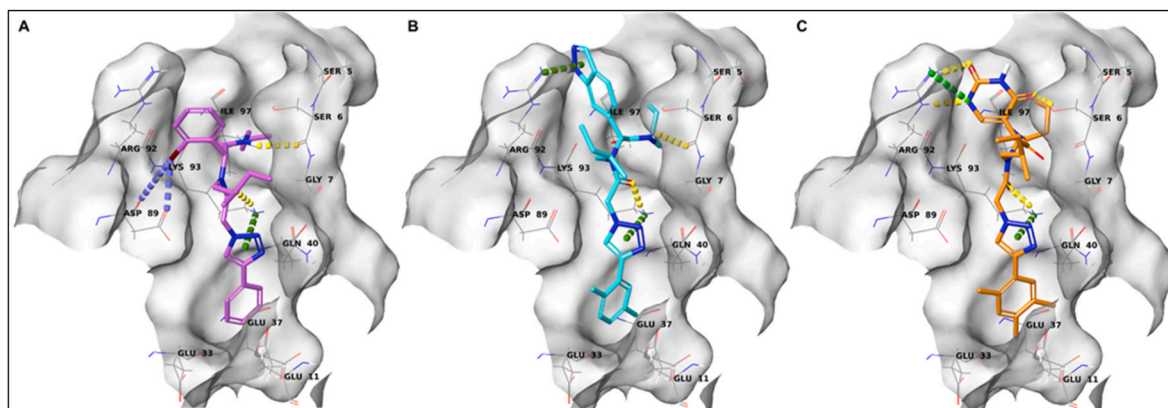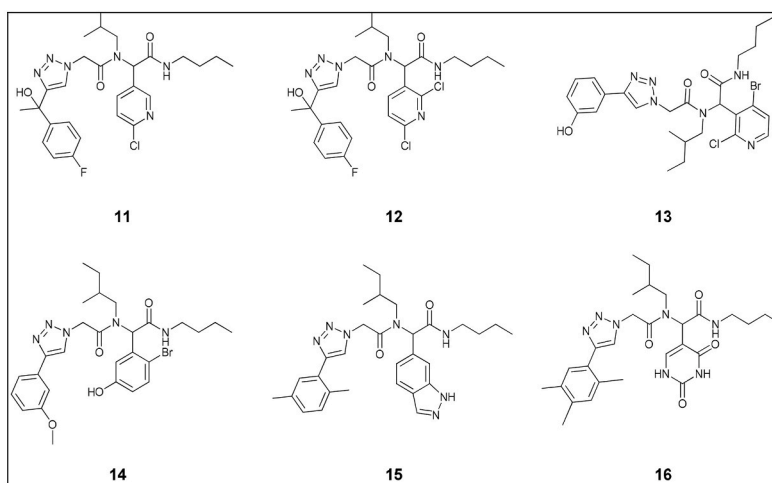
Fig. 5. Binding mode of (**a**) compound **7** (colored by atom type: C light purple, O red, N blue), (**b**) compound **15** (colored by atom type: C cyan, O red, N blue), (**c**) compound **16** (colored by atom type: C orange, O red, N blue, polar H white). H bonds, halogen bonds, and π interactions are reported in yellow, faded blue and green dotted lines, respectively. (For interpretation of the references to color in this figure legend, the reader is referred to the Web version of this article.)

Entry	R₁	R₂	R₃	R₄
11	C_6H_4ClNO (**m**)	$CH_3(CH_2)_3NC$ (**c**)	$CH_3CH_2CH(CH_3)CH_2NH_2$ (**g**)	$C_{10}H_9FO$ (**t**)
12	$C_6H_3Cl_2NO$ (**n**)	$CH_3(CH_2)_3NC$ (**c**)	$CH_3CH_2CH(CH_3)CH_2NH_2$ (**g**)	$C_{10}H_9FO$ (**t**)
13	$C_6H_3BrClNO$ (**o**)	$CH_3(CH_2)_3NC$ (**c**)	$CH_3CH_2CH(CH_3)CH_2NH_2$ (**g**)	C_8H_6O (**u**)
14	$C_7H_5BrO_2$ (**p**)	$CH_3(CH_2)_3NC$ (**c**)	$CH_3CH_2CH(CH_3)CH_2NH_2$ (**g**)	C_9H_8O (**v**)
15	$C_8H_6N_2O$ (**q**)	$CH_3(CH_2)_3NC$ (**c**)	$CH_3CH_2CH(CH_3)CH_2NH_2$ (**g**)	$C_{10}H_{10}$ (**w**)
16	$C_5H_4N_2O_3$ (**r**)	$CH_3(CH_2)_3NC$ (**c**)	$CH_3CH_2CH(CH_3)CH_2NH_2$ (**g**)	$C_{11}H_{12}$ (**x**)

Fig. 6. Structures and synthesis of compounds **11**–**16** by Ugi-Huisgen reaction. Reagents and conditions: (**i**) CH_2Cl_2, rt, 48–72 h (52–95 %); (**ii**) NaN_3, K_2CO_3, DMA, rt, 4 h; (**iii**) $CuSO_4 \cdot 5H_2O$, sod. ascorbate, DMSO/tBuOH/H_2O, rt, 12 h (47–74 %).

2.6. Biophysical assays

Compounds **11**–**16** were subjected to SPR assays to assess their affinity for the target protein [25]. The results disclosed two molecules, **15** and **16**, that exhibited a remarkable affinity for the protein counterpart, with K_D values in the low micromolar range (Table 2) [24,28].

Interestingly, these data were in accordance with computational outcomes, which disclosed the ability of compounds **15** and **16** (Fig. 6) to establish a wide set of interactions with the protein counterpart in a similar way to that of the reference compound **7** (Fig. 5).

2.7. Cell viability assay

To assess the potential anticancer properties of compounds **15** and **16**, which exhibited the best binding profiles towards BAG3-BD, we evaluated their cytotoxic effects on HeLa cells at concentrations of 10

Table 2
SPR assays of compounds **11**–**16** and **LK4** on BAG3 full length and BAG3-BD and predicted binding affinities. K_D = dissociation constant; SD = standard deviation.

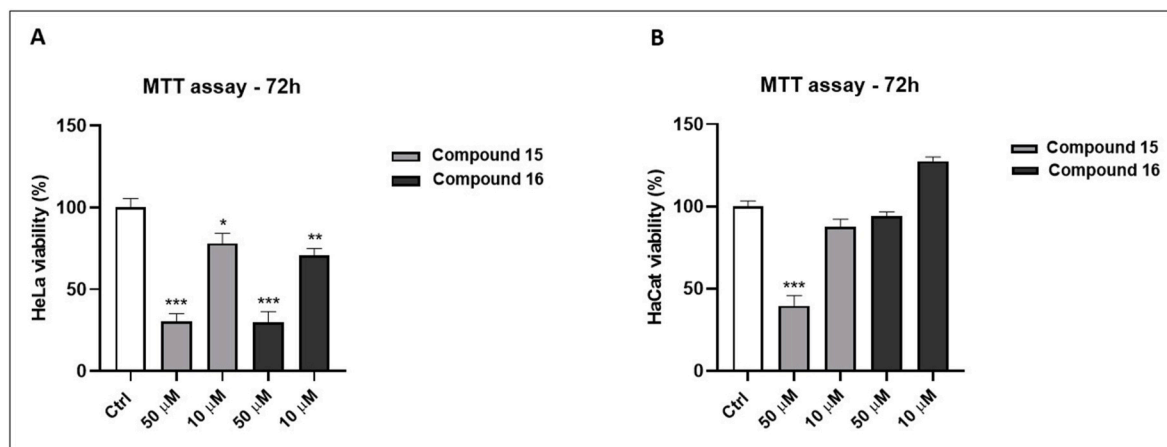| Compound	BAG3 FULL K_D (μM) ± SD	BAG-BD K_D (μM) ± SD	Docking score (kcal/mol)
11	No binding	Not determined	−6.7
12	3.62 ± 0.47	No binding	−6.4
13	No binding	Not determined	−6.4
14	No binding	Not determined	−6.3
15	4.01 ± 0.73	2.58 ± 0.17	−6.2
16	33.10 ± 5.80	27.90 ± 8.92	−6.2
LK4	19.90 ± 6.58	0.18 ± 0.02	−5.5

Fig. 7. (a) Antiproliferative activity of compounds **15** and **16** on HeLa cells after 72 h of incubation at two concentrations, 10 and 50 μM. **(b)** Antiproliferative activity of compounds **15** and **16** on HaCaT cells after 72 h of incubation at 10 and 50 μM. The control (CTRL) consisted of 0.1 % DMSO. Results are showed as mean ± standard deviation (SD) from three independent experiments. *, **, *** denote respectively $p < 0.05$; $p < 0.01$ and $p < 0.001$ vs. Ctrl.

Table 3
SPR assays of compounds **16, LK4,** and **YM-01** on BAG3 full-length, BAG3-BD, and HSP70 proteins. K_D = dissociation constant; SD = standard deviation.

Compound	BAG3 FULL K_D (μM) ± SD	BAG-BD K_D (μM) ± SD	HSP70 K_D (μM) ± SD
16	33.10 ± 5.80	27.90 ± 8.92	33.80 ± 0.14
LK4	19.90 ± 6.58	0.18 ± 0.02	No binding
YM-01	No binding	No binding	41.00 ± 9.90

and 50 μM over 72 h using an MTT proliferation assay. We chose the HeLa cell line because it demonstrated the greatest sensitivity to compound **7** in previous assays (Fig. 2). The results revealed significant cytotoxic activity of both compounds against HeLa cells, with compounds **15** and **16** causing about 70 % mortality at the same concentration (Fig. 7a) [28]. Next, we evaluated the cytotoxic effects of these promising molecules on healthy HaCaT cells (immortalized human keratinocytes) at 10 and 50 μM over 72 h. Compound **15** exhibited cytotoxicity toward healthy cells, resulting in a mortality rate of 60 % at 50 μM, while compound **16** showed no cytotoxic effects at any tested concentrations (Fig. 7b). To further ensure the safety of compound **16**, we repeated the cytotoxicity assessment on HaCaT cells at 24, 48, and 72 h, and no significant cytotoxic activity was observed in any of these instances (Fig. 7c). Consequently, our focus shifted to compound **16**, for which we calculated the IC_{50} on HeLa cells after 72 h of treatment (IC_{50}: 49.46 ± 4.96 μM).

2.8. Biophysical assays: SPR and LiP

Once an intriguing lead compound (**16**) was identified, we decided to explore its biophysical and biological properties in detail. First, we evaluated its binding affinity to HSP70, the chaperone partner of BAG3, to gain further insights into its binding profile.

Table 4
The table displays the LiP peptides identified for HSP70 and BAG3 in the interaction with **16**. For each peptide are provided the *m/z* values of the precursor (Q1) and fragment ions (Q3) and the Fold Change (Fc) values.

Q1	Q3	Protein	Peptide	Compound 16	
				Fc	p-value
844.45	694.35	Hsp70	I-[172–187]-R	2.46	0.012
658.30	910.45	Hsp70	F-[302–311]-R	1.68	0.039
707.37	214.13	Bag3	E−[461–473]-R	1.80	0.006
692.00	289.10	Bag3	Q-[451–460]-K	1.57	0.037
651.84	248.16	Bag3	Y-[150–170]-R	2.31	0.007

The assay results revealed its ability to bind HSP70 as well, highlighting its potential as a dual modulator of the BAG3-HSP70 module and as a valuable tool for discovering novel therapeutic strategies in cancer pathology. **YM-01**, a known HSP70 inhibitor, was used as a positive control (Table 3) [38].

The validation of the binding between compound **16** and its two protein counterparts, BAG3 and HSP70, was achieved by performing t-LiP (targeted-Limited Proteolysis) experiments, an MS-based proteomic technique that provides information on the binding between a protein and its ligand. This is based on the differences in resistance to the limited proteolysis of a protein target when in its free state or bound to a ligand [39]. Indeed, a ligand/protein binding can induce conformational rearrangements in the protein structure, making the protein regions affected by the binding less sensitive to the action of a protease [40]. The application of the multiple reaction monitoring mass spectrometry (MRM-MS) allows the measurement of the tryptic peptide abundances of the target protein, providing information regarding binding sites [41, 42].

In our study, the protein extract obtained from HeLa cells was incubated with compound **16** and subsequently subjected to limited proteolysis with subtilisin. A similar procedure was applied to a control sample (not treated with compound **16**). The samples were then subjected to extensive tryptic digestion for bottom-up analysis to monitor the HSP70 and BAG3 tryptic peptides coming from the two experiments. A mass method was optimized testing, on a tryptic-digested HeLa cell extract, the HSP70 and BAG3 best transitions (tryptic peptides and their fragment ions). 13 transitions for HSP70 and 13 for BAG3, giving good signals in terms of intensities and S/N ratios, were selected for the final MRM-MS experiment. A comparison of the peak intensity of each peptide in the sample treated with compound **16** and the reference one allowed the discovery of peptides with a significant fold change (peptide abundance ratio across samples) (Table 4). Specifically, two tryptic peptides were identified as involved in the binding of the molecule with HSP70 (Fig. 8a), both located in the nucleotide-binding domain (NBD). In contrast, three peptides were observed in the interaction of **16** and BAG3 (Fig. 8b), the first one is located between the two IPV regions and the other two sequential peptides are placed in the BAG domain.

Molecular docking experiments were performed to shed light on the binding of **16** towards HSP70 (see Computational Details) considering the sequence of the tryptic peptides identified through t-LiP experiments (Table 4). These highlighted the promising binding mode of **16** interacting with Arg187 through H bonds, according to the binding detected through t-LiP towards the I-[172–187]-R peptide (Fig. 9a), and with Arg311 and Glu303, through H bonds (F-[302–311]-R peptide) (Fig. 9b). Altogether, these computational outcomes corroborated the
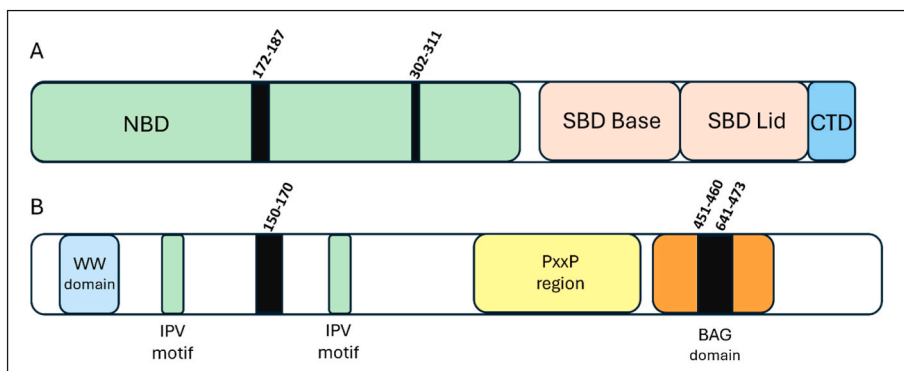
Fig. 8. The image shows graphical representations of the structures of (**a**) HSP70 and (**b**) BAG3. The black lines represent the peptides identified as involved in binding with compound **16** on the two proteins.
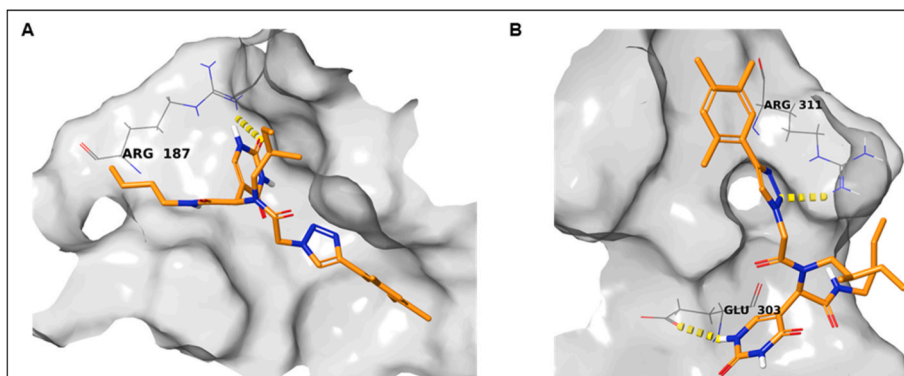

Fig. 9. (**a**) Interaction of compound **16** with the amino acids of the I-[172–187]-R peptide (colored by atom type: C orange, O red, N blue, polar H white), (**b**) interaction of compound **16** with the amino acids of the F-[302–311]-R peptide (colored by atom type: C orange, O red, N blue, polar H white). H bonds are reported in yellow dotted lines. (For interpretation of the references to color in this figure legend, the reader is referred to the Web version of this article.)

BAG3/HSP70 interference exerted by **16**.

Furthermore, with the aim to assess the stability of the protein-ligand complex and identify the main energetic and structural contributions of compound **16** with BAG3 and HSP70, molecular dynamics (MD) simulations of 1000 ns were performed. Regarding BAG3, as reported in Fig. S1a, the Root Mean Square Deviation (RMSD) of the ligand with respect to the protein and itself, supported by visual inspection of the frames of the simulation, indicated a stable protein/ligand complex throughout the whole simulation. In more details, the analysis of the RMSD of the ligand fit (purple curve in Fig. S1a) to the protein (blue curve in Fig. S1a) indicated an adaptation of **16** to the detected remarkable local flexibility of the binding site. Indeed, the analysis of the protein RMSD plots (blue curve) highlighted quite high fluctuations of the protein, but we considered this result not particularly surprising since the BAG3-BD used for the simulation feature various regions poorly structured which results in an important flexibility during the MD experiments. Furthermore, a peak in the RMSD plot of the ligand (purple curve) is detectable around 800 ns, but the visual inspection of the simulation highlighted that it is related to a movement of the ligand that follows a protein conformational change, which did not ultimately prevent the main interactions with the fundamental BAG3 amino acids. Analysis of the ligand-protein interactions (Fig. S1b) highlights that compound **16** maintains key contacts with the fundamental amino acids of the binding site reported in Fig. 5, e.g., Arg92 and Lys93, through stable H bonds (>50 % of the time).

Moreover, MD simulations were performed for HSP70 bound to **16**. In this case, the analysis of the RMSD plots and the visual inspection of the MD frames highlighted a moderate stability when the protein is bound to compound **16** (Fig. S2), which is in accordance with the fact

that, in this case, the protein structure used as input is well-structured. The observed fluctuations in the protein structure, according to the RMSD values, highlights that the binding with the ligand can determine conformational variations which can explain t-LiP results. With this aim, we also compared the results obtained from the MD simulation on HSP70-**16** complex and that performed in the absence of the ligand, with the aim of reproducing the experimental conditions of t-LiP experiments and gaining a deeper understanding of protein dynamics. The analysis of the RMSD plot for the specific peptides identified through t-LiP experiments, I-[172–187]-R and F-[302–311]-R, revealed that they exhibited distinct behaviors depending on the presence or absence of the ligand (Fig. S3). Overall, these results confirmed that the binding of HSP70 with **16** was able to determine a conformational change on the two peptides which can explain their detection from t-LiP experiments, which indeed allow the discovery of peptides with a significant fold change.

2.9. Cell cycle analysis, annexin V-FITC/PI staining, caspase 3 and caspase 9 activation

Given the known antiapoptotic functions of both BAG3 and HSP70, we evaluated the effect of compound **16** on the apoptotic response using Fluorescence-Activated Cell Sorting (FACS) analysis [43,44]. HeLa cells were incubated with various concentrations of compound **16** (10, 25, and 50 μM) and **YM-01**, a known HSP70 inhibitor (1, 5, and 10 μM), for 72 h [28]. For compound **16,** a significant increase in the apoptotic response was observed, as shown in Fig. 10a, indicated by a rise in hypodiploid nuclei compared to the negative control (cells treated with 0.1 % DMSO), with this effect being notable and consistent across the
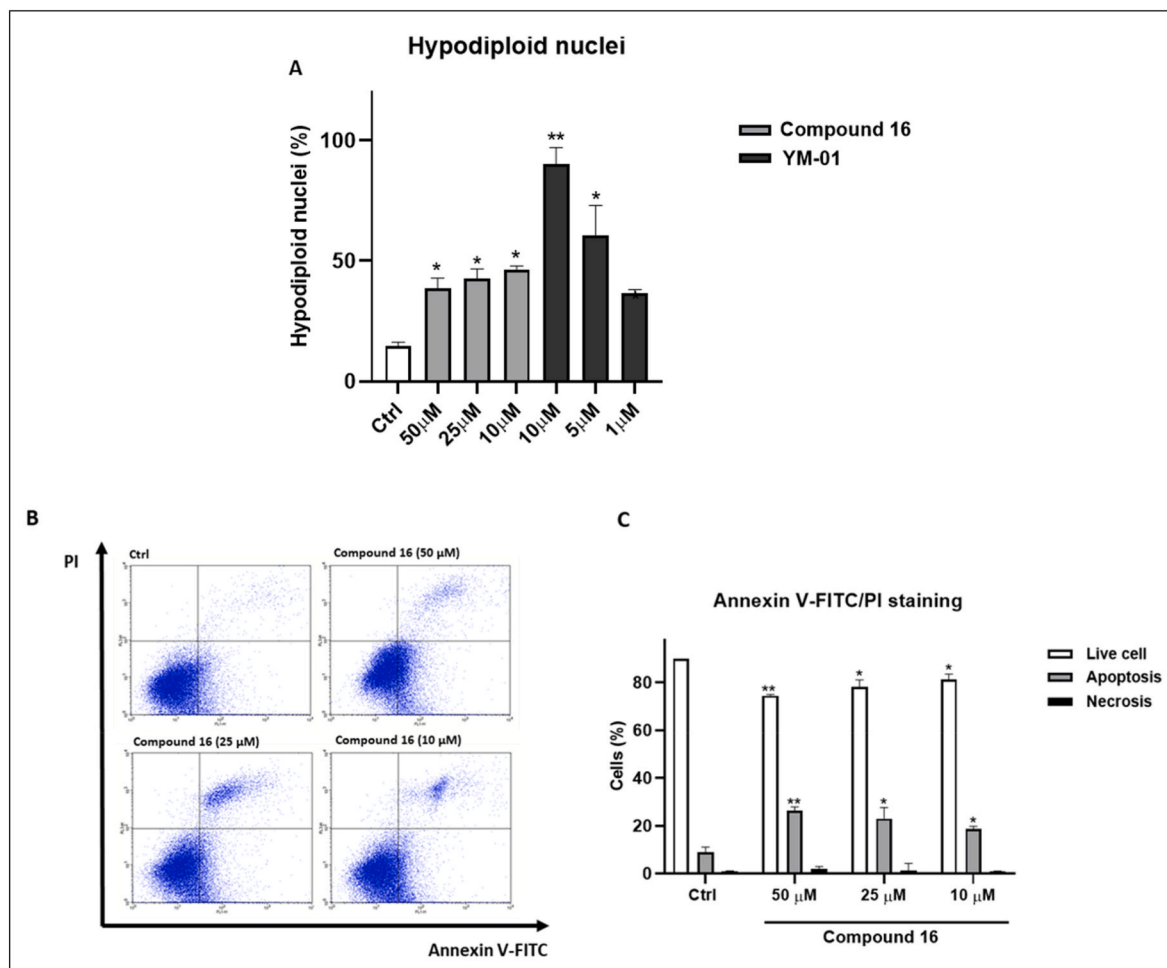
Fig. 10. (**a**) Hypodiploid nuclei were evaluated by flow cytometric analysis. HeLa cells were treated respectively with **16** (10-25-50 μM) and **YM-01** (10 μM) both for 72 h. The positive control (CTRL POS) consisted of 10 % DMSO, while the negative control (CTRL NEG) consisted of 0.1 % DMSO. (**b**) Representative flow cytometry plots using Annexin V-FITC/PI staining for apoptosis. HeLa cells were treated for 72 h with compound **16** at 50, 25, and 10 μM. (**c**) Related quantitative analysis is reported. Data are expressed as percentages of live, apoptotic, and necrotic cells. Results are shown as mean ± standard deviation (SD) from three independent experiments. *, ** denote respectively $p < 0.05$ and $p < 0.01$ vs. Ctrl.

different concentrations tested. Similarly, treatment with **YM-01** also resulted in a concentration-dependent increase in hypodiploid nuclei (Fig. 10a). To further assess the impact of compound **16** on cell apoptosis, we conducted annexin V-FITC/PI staining. The results from

FACS analysis revealed that the treatment with compound **16** led to an increase in apoptotic cells in a concentration-dependent manner, specifically within the range of 20–50 μM (50 μM: 26.2 ± 1.65 % of apoptotic cells, $p < 0.01$ vs. Ctrl; 30 μM: 23.0 ± 4.56 % of apoptotic
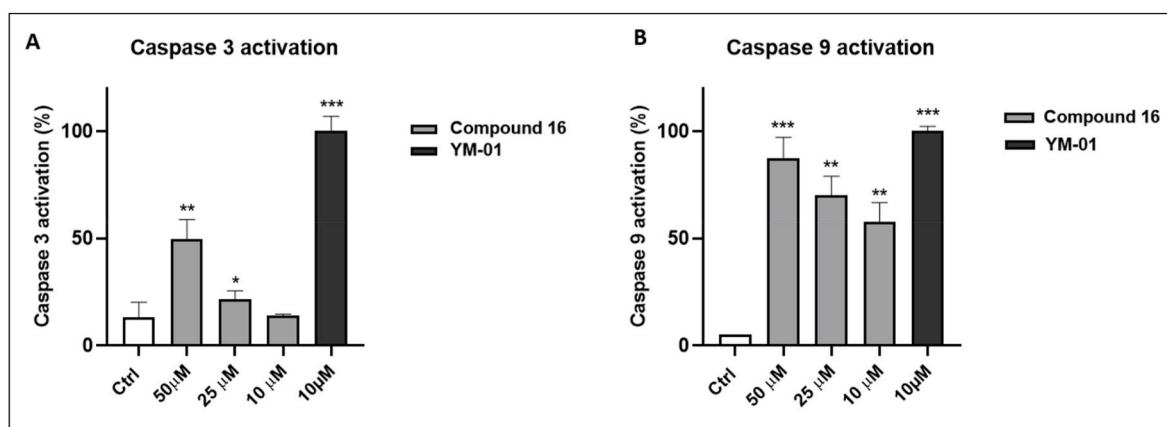
Fig. 11. (**a**) Caspase 3 and (**b**) caspase 9 expressions were evaluated by flow cytometric analysis. HeLa cells were treated respectively with **16** (10-25-50 μM) and **YM-01** (10 μM) both for 72 h. The positive control (CTRL POS) consisted of 10 % DMSO, while the negative control (CTRL NEG) consisted of 0.1 % DMSO. Results are shown as mean ± standard deviation (SD) from three independent experiments. *, **, *** denote respectively p < 0.05; p < 0.01 and p < 0.001 vs. Ctrl.

cells, $p < 0.05$ vs. Ctrl; 20 μM: 18.6 ± 1.14 % of apoptotic cells, $p < 0.05$ vs. Ctrl) (Fig. 10b and c).

Additionally, we investigated the expression of caspases, which are key mediators of programmed cell death, in HeLa cells after treatment with compound **16** at the same concentration used in the previous assay. Flow cytometry analysis revealed a significant and dose-dependent activation of both caspase 3 and caspase 9 levels in cells incubated with compound **16** compared to the control (Fig. 11a and b).

2.10. Evaluation of p21 and FOXM1 levels

Extensive research was focused on elucidating the roles of HSP70 and BAG3 in regulating key signaling proteins essential for cancer cell proliferation [45]. Several studies have shown that the depletion of HSP70 affects two critical proteins: the cell-cycle inhibitor p21 and the mitotic regulator survivin. To investigate whether BAG3 functions similarly, shRNA-mediated depletion of BAG3 was performed in various cancer cell lines. This downregulation led to a decrease in survivin levels and an accumulation of p21, closely resembling the effects observed with HSP70 depletion [46]. Furthermore, given that p21 and survivin share the same transcriptional regulator FOXM1, the HSP70–BAG3 complex influences FOXM1. Specifically, depletion of either HSP70 or BAG3 resulted in significant FOXM1 downregulation and p27 upregulation [47]. Given this background, we analyzed p21 and FOXM1 levels following treatment with compound **16**. An inhibitor targeting both proteins would elevate p21 levels while reducing FOXM1 expression. In HeLa cell experiments conducted over 72 h with compound **16** at concentrations of 10, 25, and 50 μM, we observed a dose-dependent increase in p21, suggesting a strong induction of cellular stress at this concentration. However, FOXM1 expression did not decrease correspondingly at 50 μM, in contrast to the dose-dependent effects observed at 25 and 10 μM. To ensure clarity and focus on the dose-dependent relationship, we have chosen to omit data at 50 μM for FOXM1, as the results at this concentration may reflect off-target or non-specific effects rather than the primary mechanism of action (Fig. 12).

2.11. HSP70 ATPase activity

It is well established that the ATPase activity of HSP70 allows it to cycle between different conformational states, facilitating the binding and release of client proteins. When ATP binds to the nucleotide-binding domain of HSP70, the protein adopts an open conformation that permits substrate binding. Conversely, hydrolysis of ATP to ADP induces a conformational change that promotes substrate release. The exchange between ADP and ATP at the nucleoside binding site resets the cycle,

allowing HSP70 to continue its chaperone activity. This ATP-dependent cycle is crucial for HSP70's role in assisting protein folding, preventing protein aggregation, and facilitating protein trafficking, thereby maintaining cellular proteostasis and promoting cell survival under stressful conditions [48–50].

The ADP-Glo Assay is a specialized biochemical assay used to quantify the production of adenosine diphosphate (ADP) resulting from ATP hydrolysis. The ADP-Glo Assay execution involves two main steps: first, the enzyme of interest (HSP70) catalyzes the hydrolysis of ATP to produce ADP. Then, a detection reagent is added to the reaction mixture to reconvert the generated ADP into ATP which, in turn, reacts with a luciferase enzyme and luciferin substrate to generate luminescence. The intensity of the luminescent signal is directly proportional to the amount of ADP generated, allowing for the quantification of ATP hydrolysis activity. **YM-01** was used as positive control [28]. Our findings revealed that compound **16** decreased ATPase activity by 20 % and 40 % compared to the untreated control at 10 and 50 μM concentrations, respectively. Notably, this reduction in activity closely resembled that observed with the established inhibitor **YM-01**, which showed a decrease in ATPase activity of 30 % and 43 % at 10 and 50 μM respectively (Fig. 13).

Finally, we investigated the impact of the challenging structural
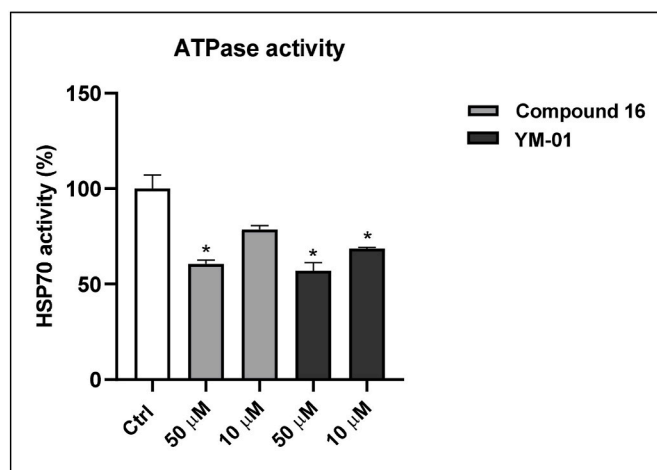
Fig. 13. Residual percentage of ATPase activity following treatment with compounds **16** and **YM-01** at two concentrations (10 and 50 μM). Results are shown as mean ± standard deviation (SD) from three independent experiments. * denotes $p < 0.05$ vs. Ctrl.
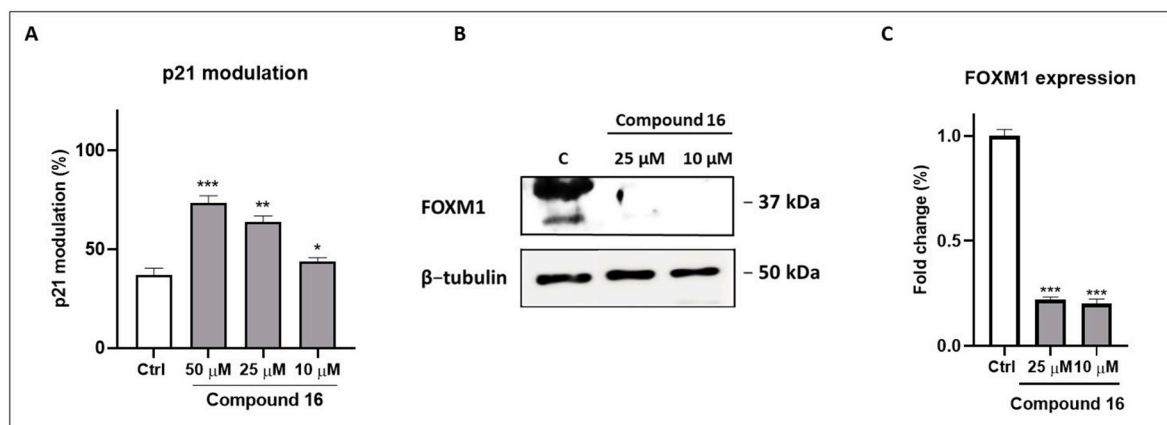
Fig. 12. (**a**) HeLa cells were treated with **16** (10-25-50 μM) for 72 h. The expression of p21 was detected by flow cytometric analysis. (**b**) HeLa cells were treated with **16** (30 and 15 μM) for 72 h. The expression of FOXM1 was detected by Western Blotting. (**c**) Related densitometric analysis is reported. Results are shown as mean ± standard deviation (SD) from three independent experiments. *, **, *** denote respectively $p < 0.05$, $p < 0.01$ and $p < 0.001$ vs. Ctrl. Ctrl consisted of 0.1 % DMSO.

features of 1,2,3-triazole-α-acylaminocarbossamide-based compounds, which present several issues. Focusing on the hit compound **16** as a reference, featuring two stereogenic centers, we attempted to separate the four related possible stereoisomers, specifically two diastereomeric racemates. Unfortunately, we were unsuccessful despite trying various elution systems, partly due to the presence of amide bond rotamers (**See** Supporting Information, Fig. S4). Indeed, the analysis of the proton spectrum reveals the presence of split signals, as seen, for example, in the case of methyne proton of asymmetric carbon generated by Ugi-reaction, which appears as two singlets [51]. We speculated whether these signals might correspond to the two different diastereoisomers or arose from a rotameric equilibrium. However, the behavior of the compound in HPLC (where its injection resulted in two broadened peaks that, once collected separately and re-injected, showed the same profile as the starting compound) together with variable-temperature NMR spectra that showed the two singlets merging into one, allowed us to confirm the presence of rotamers.

Nevertheless, the retrospective analysis of the docking poses of each stereoisomer indicated a similar binding mode (**See** Supporting Information, Fig. S5). To obtain experimental confirmation, we synthesized compound **16** using a commercially available amine with a defined configuration, thereby reducing the possible solutions to only two stereoisomers (**See** Supporting Information, Figs. S6–S10). These were then analyzed in the binding towards BAG3 via SPR, revealing a binding profile comparable to that of the original mixture (**See** Supporting Information, Table S1, and Figs. S11–S13), as expected. Based on these findings, we concluded that pursuing asymmetric synthesis was unnecessary at this stage.

3. Conclusion

In this study, through a combination of biophysical analysis, biochemical assays, and cell-based investigations, we succeeded in identifying the first molecular entity that functions as a dual modulator of BAG3 and HSP70 chaperone, two aberrantly expressed proteins in cancer cells, crucial for oncogenesis. Compound **16,** obtained using a sequential tandem reaction approach, combining the multicomponent Ugi reaction with the alkyne-azide Huisgen procedure, emerges as a compelling drug prototype with the potential to open new avenues for cancer treatment. Given that multiple signal transduction networks are often disrupted in cancer, therapies that can simultaneously modulate multiple pathways may provide more effective interventions. Furthermore, we believe that the new mechanism of action exhibited by our lead compound will enhance our understanding of the BAG3/HSP70 axis and guide future research for the discovery of a new class of potent anticancer drug candidates, as well as expanding the limited arsenal of molecules capable of modulating the two main factors of the Proteostasis Machinery.

4. Material and methods

4.1. Synthetic procedure

All starting materials and solvents used in this study were procured from Merck (Darmstadt, Germany) or Fluorochem (Hadfield, United Kingdom). NMR spectra (^{1}H, ^{13}C) were recorded on Bruker Avance instruments with field strengths of 400, 500, and 600 MHz, at a temperature of 298 K (Bruker, Milan, Italy). The compounds were dissolved in 0.5 mL of CD$_3$OD, CDCl$_3$, or (CD$_3$)$_2$SO (Merck, 99.8 Atom %D). Coupling constants (J) are reported in Hertz, and chemical shifts are expressed in parts per million (ppm) on the delta (δ) scale, with the solvent peak serving as the internal reference. Multiplicities are indicated as follows: s for singlet, d for doublet, dd for doublet of doublets, ddd for the doublet of doublet of doublets, t for triplet, dt for doublet of triplets, q for quartet, and m for multiplet. Mass spectrometry experiments were conducted using an LTQ Orbitrap XL mass spectrometer (Thermo

Scientific™, Monza, Italy). Reactions were monitored on silica gel 60 F254 plates (Merck), and the spots were visualized under UV light (λ = 254 nm, 365 nm). Semi-preparative reversed-phase HPLC was performed on an Agilent Technologies 1200 Series high-performance liquid chromatography using a Synergi Fusion, C18 reversed-phase column (250 × 10.0 mm, 4 μm, 80 Å, flow rate = 4 mL/min Phenomenex). The binary solvent system (A/B) comprised 0.1 % TFA in water (A) and 0.1 % TFA in CH$_3$CN (B), with absorbance detected at 240 nm. All biologically tested compounds were confirmed to be >98 % pure by HPLC analysis and NMR data (**See** Supporting Information, Figs. S14–S85).

4.1.1. General procedure (A) for the synthesis of intermediates I

An equimolar quantity of aldehydes **a,b,m-r** (1 equiv) and anilines **e-i** (1 equiv) were combined in dichloromethane (2 mL) and stirred at room temperature for 30 min, resulting in the formation of the Schiff base. Subsequently, isocyanides **c, d** (1 equiv) and chloroacetic acid (1 equiv) were introduced to the mixture and stirred at room temperature. The reaction's progress was monitored via TLC and found to be complete after 48–72 h. The solvent was then removed under vacuum and the resulting crude products were washed with petroleum ether (3 x 25 mL) to yield pure products **I**. These products were utilized without further purification in the subsequent step. For the intermediate intermediate **I (c,g,q)** an additional purification step by silica column chromatography (PE-EA) was performed [34].

4.1.2. N-benzyl-N-(1-(2-bromophenyl)-2-(butylamino)-2-oxoethyl)-2-chloroacetamide – intermediate I (a,c,e)

Intermediate **I (a,c,e)** was obtained by following the general procedure (**A**), from the reaction between chloroacetic acid**,** 2-bromobenzaldehyde (**a**), butyl isocyanide (**c**), and benzylamine (**e**), as white powder (194.9 mg, 80 % yield).

^{1}**H NMR** (400 MHz, CD$_3$OD): δ 7.43 (t, J = 8.6 Hz, 2H), 7.30 (t, J = 7.6 Hz, 1H), 7.19–7.09 (m, 4H), 7.05 (d, J = 7.5 Hz, 2H), 6.45 (s, 1H), 4.81 (d, J = 19.9 Hz, 1H), 4.67 (d, J = 18.0 Hz, 1H), 4.38 (d, J = 13.8 Hz, 1H), 4.21 (d, J = 13.8 Hz, 1H), 3.28–3.19 (m, 1H), 3.18–3.08 (m, 1H), 1.51–1.41 (m, 2H), 1.37–1.25 (m, 2H), 0.92 (t, J = 7.3 Hz, 3H).

4.1.3. N-benzyl-N-(1-(2-bromophenyl)-2-oxo-2-((tosylmethyl)amino) ethyl)-2-chloroacetamide – intermediate I (a,d,e)

Intermediate **I (a,d,e)** was obtained by following the general procedure (**A**), from the reaction between chloroacetic acid**,** 2-bromobenzaldehyde (**a**), 1-((isocyanomethyl)sulfonyl)-4-methylbenzene (**d**) and benzylamine (**e**), as white powder (256.6 mg, 84 % yield).

^{1}**H NMR** (400 MHz, CD$_3$OD): δ 9.21 (s, 1H), 7.71 (d, J = 8.0 Hz, 2H), 7.49–7.34 (m, 3H), 7.29 (d, J = 4.5 Hz, 2H), 7.19–7.08 (m, 3H), 6.97 (d, J = 7.0 Hz, 2H), 6.51 (s, 1H), 4.71 (d, J = 18.0 Hz, 1H), 4.63–4.41 (m, 3H), 4.33 (d, J = 13.9 Hz, 1H), 4.15 (d, J = 13.6 Hz, 1H), 2.45 (s, 3H).

4.1.4. 2-(2-bromophenyl)-N-butyl-2-(2-chloro-N-(4-chlorophenyl) acetamido)acetamide – intermediate I (a,c,f)

Intermediate **I (a,c,f)** was obtained by following the general procedure (**A**), from the reaction between chloroacetic acid**,** 2-bromobenzaldehyde (**a**), butyl isocyanide (**c**), and 4-chloroaniline (**f**), as a white powder (446 mg, 88 % yield).

^{1}**H NMR** (400 MHz, CD$_3$OD): δ 8.41 (s, 1H), 7.89 (d, J = 22.6 Hz, 1H), 7.58 (dd, J = 7.5, 1.7 Hz, 1H), 7.28 (s, 2H), 7.15–7.05 (m, 2H), 6.95 (dd, J = 7.5, 2.0 Hz, 1H), 6.48 (s, 1H), 4.05–3.90 (m, 2H), 3.31–3.18 (m, 2H), 1.55–1.45 (m, 2H), 1.39–1.27 (m, 2H), 0.93 (t, J = 7.3 Hz, 3H).

4.1.5. 2-(2-bromophenyl)-N-butyl-2-(2-chloro-N-(2-methylbutyl) acetamido)acetamide – intermediate I (a,c,g)

Intermediate **I (a,c,g)** was obtained by following the general procedure (**A**), from the reaction between chloroacetic acid**,** 2-bromobenzaldehyde (**a**), butyl isocyanide (**c**), and 2-methylbutan-1-amine (**g**), as a white powder (413.9 mg, 89 % yield).

^{1}**H NMR** (400 MHz, CD$_3$OD): δ 7.72 (d, J = 8.0 Hz, 1H), 7.45 (dd, J =

8.6, 5.1 Hz, 2H), 7.34 (t, *J* = 7.7 Hz, 1H), 6.12 (d, *J* = 13.0 Hz, 1H), 4.45–4.32 (m, 2H), 3.28–3.14 (m, 3H), 3.05 (dd, *J* = 15.7, 6.7 Hz, 1H), 1.48 (q, *J* = 7.4 Hz, 2H), 1.40–1.29 (m, 3H), 1.24 (dt, *J* = 12.7, 7.4 Hz, 1H), 1.10 (d, *J* = 7.1 Hz, 1H), 0.93 (t, *J* = 7.3 Hz, 3H), 0.75 (dd, *J* = 11.4, 6.4 Hz, 3H), 0.67 (t, *J* = 7.3 Hz, 3H).

4.1.6. N-butyl-2-(2-chloro-N-(2-hydroxyethyl)acetamido)-2-(4-(trifluoromethyl)phenyl)acetamide –intermediate I (b,c,h)

Intermediate **I (b,c,h)** was obtained by following the general procedure (**A**), from the reaction between chloroacetic acid, 4-(trifluoromethyl)benzaldehyde (**b**), butyl isocyanide (**c**) and 2-aminoethan-1-ol (**h**), as a yellowish powder (114.3 mg, 63 % yield).

^{1}H NMR (400 MHz, CD$_3$OD): δ 7.72 (d, *J* = 8.1 Hz, 1H), 7.65 (d, *J* = 8.1 Hz, 2H), 7.58 (d, *J* = 8.1 Hz, 1H), 5.89 (s, 1H), 5.07 (m, 1H), 4.56–4.46 (m, 2H), 3.56 (m, 1H), 3.35 (m, 2H), 3.22 (m, 2H), 1.50 (m, 2H), 1.41–1.34 (m, 2H), 0.92 (t, *J* = 6.7 Hz, 3H).

4.1.7. N-butyl-2-(2-chloro-N-propylacetamido)-2-(4-(trifluoromethyl) phenyl)acetamide – intermediate I (b,c, i)

Intermediate **I (b,c, i)** was obtained by following the general procedure (**A**), from the reaction between chloroacetic acid, 4-(trifluoromethyl)benzaldehyde (**b**), butyl isocyanide (**c**) and propylamine (**i**), as a white powder (133.2 mg, 85 % yield).

^{1}H NMR (400 MHz, CDCl$_3$): δ 7.66 (d, *J* = 8.0 Hz, 2H), 7.55 (d, *J* = 8.0 Hz, 2H), 5.68 (s, 1H), 4.25–4.11 (m, 2H), 3.37 (t, *J* = 8.1 Hz, 2H), 3.32–3.26 (m, 2H), 1.64–1.55 (m, 2H), 1.50–1.44 (m, 2H), 1.39–1.30 (m, 2H), 0.93 (t, *J* = 7.6 Hz, 3H), 0.82 (t, *J* = 7.3 Hz, 3H).

4.1.8. N-butyl-2-(2-chloro-N-(2-methylbutyl)acetamido)-2-(6-chloropyridin-3-yl)acetamide – intermediate I (c,g,m)

Intermediate **I (c,g,m)** was obtained by following the general procedure (**A**), from the reaction between chloroacetic acid, butyl isocyanide (**c**), 2-methylbutan-1-amine (**g**), and 6-chloronicotinaldehyde (**m**), as a yellowish powder (209.7 mg, 76 % yield).

^{1}H NMR (400 MHz, CDCl$_3$): δ 8.36 (dd, *J* = 5.4, 2.6 Hz, 1H), 7.81 (ddd, *J* = 10.9, 8.3, 2.6 Hz, 1H), 7.34 (d, *J* = 8.3 Hz, 1H), 6.47 (d, *J* = 19.3 Hz, 1H), 5.28–5.15 (m, 1H), 4.21–4.07 (m, 2H), 3.39–3.14 (m, 4H), 1.71–1.60 (m, 1H), 1.53–1.41 (m, 2H), 1.32–1.23 (m, 2H), 1.15–1.97 (m, 2H), 0.93–0.84 (m, 9H).

4.1.9. N-butyl-2-(2-chloro-N-(2-methylbutyl)acetamido)-2-(2,6-dichloropyridin-3-yl)acetamide – intermediate I (c,g,n)

Intermediate **I (c,g,n)** was obtained by following the general procedure (**A**), from the reaction between chloroacetic acid, butyl isocyanide (**c**), 2-methylbutan-1-amine (**g**), and 2,6-dichloronicotinaldehyde (**n**), as yellowish powder (228 mg, 95 % yield).

^{1}H NMR (400 MHz, CD$_3$OD): δ 7.90 (d, *J* = 8.3 Hz, 1H), 7.52 (d, *J* = 8.2 Hz, 1H), 5.80 (d, *J* = 7.7 Hz, 1H), 4.46–4.33 (m, 2H), 3.29–3.11 (m, 3H), 1.55–1.42 (m, 2H), 1.41–1.21 (m, 4H), 1.20–1.00 (m, 2H), 0.93 (t, *J* = 6.8 Hz, 3H). 0.84–0.66 (m, 6H).

4.1.10. 2-(4-Bromo-2-chloropyridin-3-yl)-N-butyl-2-(2-chloro-N-(2-methylbutyl)acetamido)acetamide – intermediate I (c,g,o)

Intermediate **I (c,g,o)** was obtained by following the general procedure (**A**), from the reaction between chloroacetic acid, butyl isocyanide (**c**), 2-methylbutan-1-amine (**g**), and 4-bromo-2-chloronicotinaldehyde (**o**), as yellowish powder (122 mg, 58 % yield).

^{1}H NMR (400 MHz, CD$_3$OD): δ 8.27 (d, *J* = 3.8 Hz, 1H), 7.79 (d, *J* = 3.8 Hz, 1H), 6.73 (s, 1H), 4.57–4.41 (m, 2H), 3.53–3.40 (m, 2H), 3.26–3.13 (m, 2H), 1.55–1.47 (m, 2H), 1.44–1.29 (m, 4H), 1.19–1.06 (m, 1H), 0.97–0.92 (t, *J* = 7.6 Hz, 3H), 0.88–0.76 (m, 3H), 0.75–0.68 (m, 3H).

4.1.11. 2-(2-Bromo-5-hydroxyphenyl)-N-butyl-2-(2-chloro-N-(2-methylbutyl)acetamido)acetamide – intermediate I (c,g,p)

Intermediate **I (c,g,p)** was obtained by following the general

procedure (**A**), from the reaction between chloroacetic acid, butyl isocyanide (**c**), 2-methylbutan-1-amine (**g**), and 2-bromo-5-hydroxybenzaldehyde (**q**), as a yellowish powder (139.9 mg, 63 % yield).

^{1}H NMR (400 MHz, (CD$_3$)$_2$SO): δ 9.88 (s, 1H), 7.83 (s, 1H), 7.42 (d, *J* = 5.0 Hz, 1H), 6.84 (dd, *J* = 5.8, 3.0 Hz, 1H), 6.74–6.70 (m, 1H), 5.92 (s, 1H), 4.45–4.38 (m, 2H), 3.19–3.02 (m, 4H), 1.41–1.34 (m, 3H), 1.31–1.23 (m, 3H), 0.92–0.83 (m, 9H).

4.1.12. N-butyl-2-(2-chloro-N-(2-methylbutyl)acetamido)-2-(1H-indazol-6-yl)acetamide – intermediate I (c,g,q)

Intermediate **I (c,g,q)** was obtained by following the general procedure (**A**), from the reaction between chloroacetic acid, butyl isocyanide (**c**), 2-methylbutan-1-amine (**g**), and 1H-indazole-6-carbaldehyde (**r**), as a white powder (131.6 mg, 52 % yield).

^{1}H NMR (400 MHz, CDCl$_3$): δ 8.03 (s, 1H), 7.71 (d, *J* = 8.3 Hz, 2H), 7.13–7.08 (m, 1H), 6.39 (s, 1H), 4.30–4.17 (m, 2H), 3.33–3.18 (m, 4H), 1.45–1.34 (m, 3H), 1.27–1.19 (m, 3H), 1.01–0.94 (m, 1H), 0.86–0.70 (m, 9H)

4.1.13. N-butyl-2-(2-chloro-N-(2-methylbutyl)acetamido)-2-(2,4-dioxo-1,2,3,4-tetrahydropyrimidin-5-yl)acetamide intermediate I (c,g,r)

Intermediate **I (c,g,r)** was obtained by following the general procedure (**A**), from the reaction between chloroacetic acid, butyl isocyanide (**c**), 2-methylbutan-1-amine (**g**), and 5-formyluracil (**r**), as yellowish-white oil (409.5 mg, 64 % yield).

^{1}H NMR (400 MHz, CDCl$_3$): δ 9.35 (s, 1H), 7.91 (s, 1H), 6.67 (s, 1H), 5.11 (d, *J* = 16 Hz, 1H), 4.14 (s, 2H), 3.54–3.19 (m, 4H), 1.83–1.71 (m, 1H), 1.53–1.41 (m, 2H), 1.38–1.23 (m, 2H), 1.17–1.02 (m, 2H), 1.01–0.77 (m, 9H).

4.1.14. General procedure (B) for the synthesis of intermediates II

Equimolar quantities of the respective Ugi chloride **I** (1 equiv) and sodium azide (1 equiv) were combined in dimethyl acetamide (1 mL). Subsequently, K$_2$CO$_3$ (2.88 equiv) was added to the mixture, which was stirred at room temperature for 4 h. The resulting reaction mixture was then diluted with water, leading to the formation of a white precipitate that was filtered and washed repeatedly with water to obtain pure azides **II**. If no precipitate is formed, the aqueous layer is extracted with ethyl acetate (3 × 50ml). These products were utilized without further purification in the subsequent step [34].

4.1.15. 2-Azido-N-benzyl-N-(1-(2-bromophenyl)-2-(butylamino)-2-oxoethyl)acetamide – intermediate II (a,c,e)

Intermediate **II (a,c,e)** was obtained by following the general procedure (**B**) starting from intermediate **I (a,c,e)**, as white powder after precipitation (76.7 mg, 98 % yield).

^{1}H NMR (400 MHz, CDCl$_3$): δ 7.63–7.55 (m, 1H), 7.49 (dd, *J* = 8.0, 1.2 Hz, 1H), 7.28 (s, 1H), 7.22–7.09 (m, 4H), 7.07–7.00 (m, 2H), 6.36 (s, 1H), 5.72 (s, 1H), 4.59 (s, 2H), 3.98 (d, *J* = 16.0 Hz, 1H), 3.77 (d, *J* = 16.0 Hz, 1H), 3.28 (d, *J* = 16.7 Hz, 2H), 1.54–1.42 (m, 2H), 1.37–1.24 (m, 2H), 0.92 (t, *J* = 7.3 Hz, 3H).

4.1.16. 2-Azido-N-benzyl-N-(1-(2-bromophenyl)-2-oxo-2-((tosylmethyl) amino)ethyl)acetamide – intermediate II (a,d,e)

Intermediate **II (a,d,e)** was obtained by following the general procedure (**B**) starting from intermediate **I (a,d,e)**, as a white powder after precipitation (171.2 mg, 68 % yield).

^{1}H NMR (400 MHz, CD$_3$OD): δ 9.22 (t, *J* = 6.6 Hz, 1H), 7.82–7.66 (m, 2H), 7.53–7.37 (m, 3H), 7.29 (d, *J* = 4.5 Hz, 2H), 7.19–7.04 (m, 3H), 6.95 (t, *J* = 11.5 Hz, 2H), 6.56 (s, 1H), 4.60 (dd, *J* = 19.4, 7.1 Hz, 2H), 4.43 (d, *J* = 18.3 Hz, 1H), 4.20–4.06 (m, 2H), 3.82 (d, *J* = 16.4 Hz, 1H), 2.45 (s, 3H).

4.1.17. 2-Azido-N-(1-(2-bromophenyl)-2-(butylamino)-2-oxoethyl)-N-(4-chlorophenyl)acetamide – intermediate II (a,c,f)

Intermediate **II (a,c,f)** was obtained by following the general

procedure (**B**) starting from the intermediate **I (a,c,f),** as yellowish-white powder after precipitation (374.1 mg, 83 % yield).

¹H NMR (400 MHz, (CD₃)₂SO): δ 8.38 (q, *J* = 9.7, 7.7 Hz, 1H), 7.61–7.51 (m, 1H), 7.36–7.03 (m, 5H), 6.89–6.81 (m, 1H), 6.29 (s, 1H), 3.86 (d, *J* = 16.5 Hz, 1H), 3.59 (d, *J* = 16.5 Hz, 1H), 3.25–3.13 (m, 1H), 3.12–3.04 (m, 1H), 1.43–1.34 (m, 2H), 1.30–1.16 (m, 2H), 0.85 (t, *J* = 7.3 Hz, 3H).

4.1.18. 2-Azido-N-(1-(2-bromophenyl)-2-(butylamino)-2-oxoethyl)-N-(2-methylbutyl)acetamide – intermediate II (a,c,g)

Intermediate **II (a,c,g)** was obtained by following the general procedure (**B**) starting from the intermediate **I (a,c,g),** as white powder after precipitation (200 mg, 49 % yield).

¹H NMR (400 MHz, (CD₃)₂SO): δ 8.16 (q, *J* = 6.2 Hz, 1H), 7.74–7.65 (m, 1H), 7.48–7.39 (m, 1H), 7.37–7.30 (m, 2H), 6.04 (d, *J* = 16.2 Hz, 1H), 4.29–3.92 (m, 2H), 3.41 (d, *J* = 9.6 Hz, 1H), 3.22–2.96 (m, 3H), 2.90–2.79 (m, 1H), 1.44–1.33 (m, 2H), 1.31–1.18 (m, 2H), 1.09 (dd, *J* = 14.5, 7.1 Hz, 1H), 0.94–0.76 (m, 4H), 0.64 (d, *J* = 6.6 Hz, 3H), 0.59–0.48 (m, 3H).

4.1.19. 2-Azido-N-(2-(butylamino)-2-oxo-1-(4-(trifluoromethyl)phenyl)ethyl)-N-(2-hydroxyethyl)acetamide –intermediate II (b,c,h)

Intermediate **II (b,c,h)** was obtained by following the general procedure (**B**) starting from the intermediate **I (b,c,h),** as yellowish white oil after extraction (29.7 mg, 24 % yield).

¹H NMR (400 MHz, CD₃OD): δ 7.68 (m, 4H), 5.17 (s, 1H), 4.36–4.27 (m, 2H), 4.11–3.86 (m, 2H), 3.26–3.19 (m, 4H), 1.50 (m, 2H), 1.40–1.31 (m, 2H), 0.92 (t, *J* = 6.7 Hz, 3H).

4.1.20. 2-Azido-N-(2-(butylamino)-2-oxo-1-(4-(trifluoromethyl)phenyl)ethyl)-N-propylacetamide – intermediate II (b,c, i)

Intermediate **II (b,c, i)** was obtained by following the general procedure (**B**) starting from intermediate **I (b,c, i),** as a white powder after precipitation (92.2 mg, 68 % yield).

¹H NMR (400 MHz, (CD₃)₂SO): δ 7.74 (d, *J* = 8.0 Hz, 2H), 7.48 (d, *J* = 8.0 Hz, 2H), 5.98 (s, 1H), 4.29–4.13 (m, 2H), 3.25–3.01 (m, 4H), 1.64–1.55 (m, 2H), 1.42–1.32 (m, 2H), 1.30–1.23 (m, 2H), 1.23–1.22 (m, 2H), 0.84 (t, *J* = 7.6 Hz, 3H), 0.56 (t, *J* = 6.7 Hz, 3H).

4.1.21. 2-Azido-N-(2-(butylamino)-1-(6-chloropyridin-3-yl)-2-oxoethyl)-N-(2-methylbutyl)acetamide –intermediate II (c,g,m)

Intermediate **II (c,g,m)** was obtained by following the general procedure (**B**) starting from the intermediate **I (c,g,m),** as a yellowish powder after precipitation (141.7 mg, 69 % yield).

¹H NMR (400 MHz, CDCl₃): δ 8.33 (dd, *J* = 4.1, 2.6 Hz, 1H), 7.83 (ddd, *J* = 8.7, 6.4, 2.6 Hz, 1H), 7.33 (d, *J* = 8.3 Hz, 1H), 6.50 (s, 1H), 5.34 (d, *J* = 27.1 Hz, 1H), 3.97 (d, *J* = 3.8 Hz, 2H), 3.29–3.13 (m, 3H), 3.11–3.03 (m, 1H), 1.49–1.39 (m, 3H), 1.35–1.20 (m, 3H), 1.05–0.93 (m, 1H), 0.90–0.75 (m, 9H).

4.1.22. 2-Azido-N-(2-(butylamino)-1-(2,6-dichloropyridin-3-yl)-2-oxoethyl)-N-(2-methylbutyl)acetamide –intermediate II (c,g,n)

Intermediate **II (c,g,n)** was obtained by following the general procedure (**B**) starting from the intermediate **I (c,g,n),** as a white powder after extraction (60 mg, 27 % yield).

¹H NMR (400 MHz, CDCl₃): δ 7.61 (d, *J* = 8.3 Hz, 1H), 7.18 (d, *J* = 8.2 Hz, 1H), 5.29 (s, 1H), 3.97–3.82 (m, 2H), 3.23–3.07 (m, 3H), 1.42–1.32 (m, 4H), 1.27–1.16 (m, 4H), 0.80 (t, *J* = 6.8 Hz, 3H), 0.76–0.66 (m, 6H).

4.1.23. 2-Azido-N-(1-(4-bromo-2-chloropyridin-3-yl)-2-(butylamino)-2-oxoethyl)-N-(2-methylbutyl)acetamide – intermediate II (c,g,o)

Intermediate **II (c,g,o)** was obtained by following the general procedure (**B**) starting from the intermediate **I (c,g,o),** as a yellowish powder after extraction (75.6 mg, 61 % yield).

¹H NMR (400 MHz, CDCl₃): δ 8.06 (d, *J* = 3.8 Hz, 1H), 7.44 (d, *J* =

3.8 Hz, 1H), 5.78 (s, 1H), 4.05–3.80 (m, 2H), 3.30–3.19 (m, 4H), 1.54–1.48 (m, 3H), 1.39–1.32 (m, 4H), 0.97–0.87 (m, 9H).

4.1.24. 2-Azido-N-(1-(2-bromo-5-hydroxyphenyl)-2-(butylamino)-2-oxoethyl)-N-(2-methylbutyl)acetamide –intermediate II (c,g,p)

Intermediate **II (c,g,p)** was obtained by following the general procedure (**B**) starting from intermediate **I (c,g,p),** as a white powder after extraction (63.2 mg, 45 % yield).

¹H NMR (400 MHz, CDCl₃): δ 7.40 (d, *J* = 8.7 Hz, 1H), 7.28 (d, *J* = 3.0 Hz, 1H), 6.79 (dd, *J* = 8.7, 2.9 Hz, 1H), 6.06 (s, 1H), 5.69 (s, 1H), 4.04 (d, *J* = 4.4 Hz, 2H), 3.33–3.21 (m, 2H), 3.20–3.07 (m, 2H), 1.45–1.35 (m, 2H), 1.29–1.20 (m, 4H), 0.86–0.79 (m, 6H), 0.66 (t, *J* = 7.2 Hz, 3H).

4.1.25. 2-Azido-N-(2-(butylamino)-1-(1H-indazol-6-yl)-2-oxoethyl)-N-(2-methylbutyl)acetamide – intermediate II (c,g,q)

Intermediate **II (c,g,q)** was obtained by following the general procedure (**B**) starting from the intermediate **I (c,g,q),** as a yellowish powder after precipitation (78.2 mg, 78 % yield).

¹H NMR (400 MHz, CDCl₃): δ 7.98 (s, 1H), 7.69–7.62 (m, 2H), 7.06 (t, *J* = 6.7 Hz, 1H), 6.41 (s, 1H), 4.02–3.93 (m, 2H), 3.32–3.11 (m, 4H), 1.43–1.30 (m, 3H), 1.24–1.15 (m, 4H), 0.87–0.75 (m, 5H), 0.66–0.58 (m, 4H).

4.1.26. 2-Azido-N-(2-(butylamino)-1-(2,4-dioxo-1,2,3,4-tetrahydropyrimidin-5-yl)-2-oxoethyl)-N-(2 methylbutyl)acetamide - intermediate II (c,g,r)

Intermediate **II (c,g,r)** was obtained by following the general procedure (**B**) starting from intermediate **I (c,g,r),** as yellow oil after extraction (235.1 mg, 84 % yield).

¹H NMR (400 MHz, CDCl₃): δ 7.86 (s, 1H), 7.04 (s, 1H), 5.20 (d, *J* = 16 Hz, 1H), 3.92 (dd, *J* = 16, 7.6 Hz, 2H), 3.21–3.04 (m, 4H), 1.65–1.54 (m, 1H), 1.41–1.33 (m, 2H), 1.28–1.17 (m, 2H), 1.04–0.90 (m, 2H), 0.85–0.77 (m, 9H).

4.1.27. General procedures (C) for the synthesis of 1–16

An equimolar quantity of alkynes **j-l, t-x** (1 equiv), and Ugi azides **II** (1 equiv) were dissolved in the minimum amount of DMSO. To this solution, 2 mL of t-BuOH, 1 mL of water, CuSO₄·5H₂O (3.2 equiv), and sodium ascorbate (3 equiv) were added. The mixture was stirred at room temperature for 12 h and then poured into cold water. The resulting precipitate was filtered, washed with water, and dried under vacuum, yielding the final products **1–16** [34].

4.1.28. N-benzyl-N-(1-(2-bromophenyl)-2-(butylamino)-2-oxoethyl)-2-(4-phenyl-1H-1,2,3-triazol-1-yl)acetamide - Compound 1

Compound **1** was obtained by following the general procedure (**C**), from the reaction between **II (a,c,e)** and ethynylbenzene (**j**), as a white powder (71.8 mg, 92 % yield after HPLC purification).

RP-HPLC t_R = 29 min, gradient condition: from 5 % B ending to 100 % B 40 min, flow rate of 4 mL/min, λ = 240 nm.

¹H NMR (400 MHz, CDCl₃) δ 8.01 (d, *J* = 6.0 Hz, 1H), 7.84 (d, *J* = 7.5 Hz, 2H), 7.55 (dd, *J* = 20.6, 7.9 Hz, 2H), 7.43 (t, *J* = 7.6 Hz, 2H), 7.34 (t, *J* = 7.4 Hz, 2H), 7.29–7.12 (m, 6H), 6.29 (s, 1H), 5.34–5.09 (m, 2H), 4.87–4.63 (m, 2H), 3.37–3.20 (m, 2H), 1.50–1.41 (m, 2H), 1.33–1.25 (m, 2H), 0.90 (t, *J* = 7.3 Hz, 3H).

¹³C NMR (101 MHz, CDCl₃): δ 168.4, 167.0, 147.9, 135.8, 133.5, 133.4, 131.1, 130.6, 130.5, 128.8, 128.7 (2C), 128.1 (2C), 128.0 (2C), 127.7, 126.5, 126.2, 125.8 (2C), 121.7, 63,2, 51.6, 49.8, 39.6, 31.3, 20.0, 13.6.

ESI-MS: calculated for C₂₉H₃₀BrN₅O₂ 559.1583; found *m/z* = 582.1431 [M + Na]⁺.

4.1.29. N-benzyl-N-(1-(2-bromophenyl)-2-(butylamino)-2-oxoethyl)-2-(4-isopentyl-1H-1,2,3-triazol-1-yl)acetamide - Compound 2

Compound **2** was obtained by following the general procedure (**C**),

from the reaction between **II (a,c,e)** and 5-methylhex-1-yne (**k**), as a white powder (107.2 mg, 78 % yield after HPLC purification).

RP-HPLC t_R = 32 min, gradient condition: from 5 % B ending to 100 % B 40 min, flow rate of 4 mL/min, λ = 240 nm.

^{1}H NMR (400 MHz, CD$_3$OD): δ 7.79 (d, J = 22.3 Hz, 1H), 7.45 (d, J = 8.1 Hz, 2H), 7.31 (t, J = 7.6 Hz, 1H), 7.24–7.09 (m, 5H), 7.04 (s, 1H), 6.88 (s, 1H), 6.47 (s, 1H), 5.52 (d, J = 16.8 Hz, 1H), 5.27 (d, J = 16.7 Hz, 1H), 4.91 (d, J = 18.3 Hz, 1H), 4.73 (d, J = 18.1 Hz, 1H), 3.29–3.20 (m, 1H), 3.19–3.09 (m, 1H), 2.75 (t, J = 7.7 Hz, 2H), 1.69–1.53 (m, 3H), 1.52–1.40 (m, 2H), 1.38–1.25 (m, 2H), 0.98 (d, J = 6.1 Hz, 6H), 0.91 (t, J = 7.3 Hz, 3H).

^{13}C NMR (101 MHz, CD$_3$OD): δ 170.0, 168.0, 147.9, 136.1, 134.0, 132.9, 130.9, 130.2, 128.1, 127.5, 127.3, 127.2, 126.9, 126.6, 125.9, 123.6, 62.2, 51.2, 48.6, 38.9, 38.2, 30.8, 27.3, 22.8, 21.3 (2C), 19.6, 12.6.

ESI-MS: calculated for C$_{28}$H$_{36}$BrN$_5$O$_2$ 553.2052; found m/z = 554.2123 [M + H]$^+$.

4.1.30. *N-benzyl-N-(1-(2-bromophenyl)-2-oxo-2-((tosylmethyl)amino) ethyl)-2-(4-phenyl-1H-1,2,3-triazol-1-yl)acetamide - Compound 3*

Compound **3** was obtained by following the general procedure (**C**), from the reaction between **II (a,d,e)** and ethynylbenzene (**j**), as a white powder (125.8 mg, 75 % yield after HPLC purification).

RP-HPLC t_R = 30 min, gradient condition: from 5 % B ending to 100 % B 40 min, flow rate of 4 mL/min, λ = 240 nm.

^{1}H NMR (400 MHz, CD$_3$OD): δ 8.31 (s, 1H), 7.84 (d, J = 8.0 Hz, 2H), 7.67 (d, J = 8.0 Hz, 1H), 7.50–7.41 (m, 4H), 7.38–7.26 (m, 5H), 7.23–7.08 (m, 6H), 6.50 (s, 1H), 5.57 (d, J = 16.9 Hz, 1H), 5.34–5.25 (m, 2H), 4.65–4.54 (m, 3H), 2.43 (s, 3H).

^{13}C NMR (101 MHz, CD$_3$OD): δ 170.3, 167.9, 147.5, 145.3, 136.0, 134.4, 133.0, 132.9, 131.6, 130.5, 130.3, 129.6 (2C), 128.6 (2C), 128.1 (2C), 128.0 (2C), 127.6, 126.9, 126.8, 125.9 (2C), 125.3 (2C), 122.8, 62.0, 60.2, 51.4, 48.5, 20.2.

ESI-MS: calculated for C$_{33}$H$_{30}$BrN$_5$O$_4$S 671.1202; found m/z = 694.1084 [M+Na]$^+$.

4.1.31. *N-benzyl-N-(1-(2-bromophenyl)-2-oxo-2-((tosylmethyl)amino) ethyl)-2-(4-isopentyl-1H-1,2,3-triazol-1-yl)acetamide - Compound 4*

Compound **4** was obtained by following the general procedure (**C**), from the reaction between **II (a,d,e)** and 5-methylhex-1-yne (**k**), as a white powder (117.8 mg, 32 % yield after HPLC purification).

RP-HPLC t_R = 31 min, gradient condition: from 5 % B ending to 100 % B 40 min, flow rate of 4 mL/min, λ = 240 nm.

^{1}H NMR (400 MHz, CD$_3$OD): δ 9.20 (t, J = 6.6 Hz, 1H), 7.81 (s, 1H), 7.74 (s, 1H), 7.69 (d, J = 8.0 Hz, 1H), 7.51–7.37 (m, 2H), 7.37–7.27 (m, 3H), 7.17 (q, J = 8.0, 7.2 Hz, 3H), 7.07 (d, J = 7.1 Hz, 1H), 6.99 (s, 1H), 6.75 (s, 1H), 6.51 (s, 1H), 5.49 (d, J = 16.9 Hz, 1H), 5.20 (d, J = 16.8 Hz, 1H), 4.79 (s, 2H), 4.57 (d, J = 17.6 Hz, 2H), 2.75 (t, J = 7.7 Hz, 2H), 2.45 (s, 3H), 1.62 (q, J = 7.8, 6.9 Hz, 3H), 0.97 (d, J = 6.0 Hz, 6H).

^{13}C NMR (101 MHz, CD$_3$OD): δ 170.3, 168.0, 145.3, 139.3, 139.1, 136.0, 134.4, 133.0, 132.9, 131.6, 130.5, 129.6 (2C), 128.6 (2C), 128.0 (2C), 127.5, 126.8, 126.7, 125.9 (2C), 61.9, 60.1, 51.3, 48.3, 38.2, 27.2, 22.8, 21.2 (2C), 20.3.

ESI-MS: calculated for C$_{32}$H$_{36}$BrN$_5$O$_4$S 665.1671; found m/z = 688.1526 [M+Na]$^+$.

4.1.32. *2-(2-bromophenyl)-N-butyl-2-(N-(4-chlorophenyl)-2-(4-phenyl-1H-1,2,3-triazol-1-yl)acetamido)acetamide - Compound 5*

Compound **5** was obtained by following the general procedure (**C**), from the reaction between **II (a,c,f)** and ethynylbenzene (**j**), as a yellowish–white powder (168.2 mg, 93 % yield after HPLC purification).

RP-HPLC t_R = 32 min, gradient condition: from 5 % B ending to 100 % B 40 min, flow rate of 4 mL/min, λ = 240 nm.

^{1}H NMR (400 MHz, (CD$_3$)$_2$SO): δ 8.47 (s, 1H), 8.38 (t, J = 5.6 Hz, 1H), 8.04 (s, 1H), 7.89–7.82 (m, 2H), 7.63–7.55 (m, 1H), 7.46 (t, J = 7.6 Hz, 2H), 7.34 (t, J = 7.4 Hz, 1H), 7.27 (t, J = 7.4 Hz, 1H), 7.18–7.08 (m,

2H), 7.08–6.96 (m, 1H), 6.94–6.85 (m, 1H), 6.29 (s, 1H), 5.20 (d, J = 17.0 Hz, 1H), 4.94 (d, J = 17.0 Hz, 1H), 3.25–3.15 (m, 1H), 3.10–2.98 (m, 1H), 1.42–1.31 (m, 2H), 1.31–1.14 (m, 2H), 0.83 (t, J = 7.3 Hz, 3H).

^{13}C NMR (101 MHz, (CD$_3$)$_2$SO): δ 168.8, 165.8, 146.5, 136.8, 134.4, 133.7, 133.1 (2C), 131.8 (2C), 131.2, 130.8 (2C), 129.4 (2C), 128.3 (2C), 127.9, 126.4, 125.6 (2C), 123.5, 64.2, 51.9, 38.9, 31.3, 19.9, 14.0.

ESI-MS: calculated for C$_{28}$H$_{27}$BrClN$_5$O$_2$ 579.1037; found m/z = 602.0882 [M+Na]$^+$.

4.1.33. *2-(2-bromophenyl)-N-butyl-2-(N-(4-chlorophenyl)-2-(4-isopentyl-1H-1,2,3-triazol-1-yl)acetamido)acetamide - Compound 6*

Compound **6** was obtained by following the general procedure (**C**), from the reaction between **II (a,c,f)** and 5-methylhex-1-yne (**k**), as a white powder (178.6 mg, 78 % yield after HPLC purification).

RP-HPLC t_R = 32 min, gradient condition: from 5 % B ending to 100 % B 40 min, flow rate of 4 mL/min, λ = 240 nm.

^{1}H NMR (400 MHz, (CD$_3$)$_2$SO): δ 8.36 (t, J = 5.6 Hz, 1H), 7.99 (s, 1H), 7.71 (s, 1H), 7.64–7.55 (m, 1H), 7.50–7.20 (m, 2H), 7.15–7.05 (m, 2H), 6.98 (d, J = 11.6 Hz, 1H), 6.92–6.80 (m, 1H), 6.26 (s, 1H), 5.06 (d, J = 16.9 Hz, 1H), 4.82 (d, J = 16.8 Hz, 1H), 3.24–3.14 (m, 1H), 3.10–2.97 (m, 1H), 2.66–2.57 (m, 2H), 1.61–1.51 (m, 1H), 1.52–1.44 (m, 2H), 1.40–1.31 (m, 2H), 1.22 (ddd, J = 14.7, 7.9, 5.9 Hz, 2H), 0.91 (d, J = 6.4 Hz, 6H), 0.84 (t, J = 7.3 Hz, 3H).

^{13}C NMR (101 MHz, (CD$_3$)$_2$SO): δ 168.9, 165.8, 147.0, 136.8, 134.5, 133.6, 133.1, 131.8, 130.8 (2C), 129.3 (2C), 127.8 (2C), 126.3, 123.7, 64.1, 51.6, 39.0, 38.6, 31.3, 27.3, 23.3, 22.7 (2C), 19.9, 14.0.

ESI-MS: calculated for C$_{27}$H$_{33}$BrClN$_5$O$_2$ 573.1506; found m/z = 596.1346 [M+Na]$^+$.

4.1.34. *2-(2-bromophenyl)-N-butyl-2-(N-(2-methylbutyl)-2-(4-phenyl-1H-1,2,3-triazol-1-yl)acetamido)acetamide - Compound 7*

Compound **7** was obtained by following the general procedure (**C**), from the reaction between **II (a,c,g)** and ethynylbenzene (**j**), as a yellowish–white powder (129.5 mg, 96 % yield after HPLC purification).

RP-HPLC t_R = 30 min, gradient condition: from 5 % B ending to 100 % B 40 min, flow rate of 4 mL/min, λ = 240 nm.

^{1}H NMR (400 MHz, (CD$_3$)$_2$SO), mixture of rotamers: δ 8.58–8.53 (m, 1H), 8.15 (q, J = 6.0 Hz, 1H), 7.92–7.86 (m, 2H), 7.79–7.69 (m, 1H), 7.49–7.42 (m, 3H), 7.39–7.31 (m, 3H), 6.02 (d, J = 18.3 Hz, 1H), 5.65–5.45 (m, 2H), 3.27–3.09 (m, 3H), 3.04–2.93 (m, 1H), 1.51–1.41 (m, 1H), 1.39–1.29 (m, 2H), 1.27–1.15 (m, 3H), 0.89 (t, J = 7.3 Hz, 1H), 0.86–0.78 (m, 3H), 0.74–0.57 (m, 6H).

^{13}C NMR (101 MHz, (CD$_3$)$_2$SO), mixture of rotamers: δ 168.9, 167.2, 146.6, 135.6, 133.6, 133.3, 131.6, 131.3, 131.0, 129.4 (2C), 128.2, 126.9, 125.6 (2C), 123.8, 62.8, 51.4 (2C), 38.9, 34.6, 31.3, 26.6, 19.9, 17.2, 14.0, 11.7.

ESI-MS: calculated for C$_{27}$H$_{34}$BrN$_5$O$_2$ 539.1896; found m/z = 562.1739 [M+Na]$^+$.

4.1.35. *2-(2-bromophenyl)-N-butyl-2-(2-(4-isopentyl-1H-1,2,3-triazol-1-yl)-N-(2-methylbutyl)acetamido)acetamide - Compound 8*

Compound **8** was obtained by following the general procedure (**C**), from the reaction between **II (a,c,g)** and 5-methylhex-1-yne (**k**), as a yellowish–white powder (90.7 mg, 86 % yield after HPLC purification).

RP-HPLC t_R = 32 min, gradient condition: from 5 % B ending to 100 % B 40 min, flow rate of 4 mL/min, λ = 240 nm.

^{1}H NMR (600 MHz, (CD$_3$)$_2$SO) δ 8.11 (s, 1H), 7.82–7.68 (m, 2H), 7.48–7.33 (m, 3H), 5.99 (dd, J = 26.6, 2.3 Hz, 1H), 5.53–5.33 (m, 2H), 3.27–2.96 (m, 4H), 2.64 (t, J = 7.9 Hz, 2H), 1.62–1.40 (m, 4H), 1.39–1.15 (m, 6H), 0.92 (dd, J = 6.5, 2.3 Hz, 8H), 0.84 (t, J = 7.4 Hz, 3H), 0.64–0.55 (m, 4H).

^{13}C NMR (151 MHz, (CD$_3$)$_2$SO), mixture of rotamers: δ 168.9, 167.3, 147.0, 135.6, 133.2, 131.6, 131.0, 128.3, 126.9, 124.0, 62.7, 51.2, 38.9, 38.6, 34.6, 31.3, 27.3, 26.6, 23.4, 22.7 (2C), 20.0, 18.0, 17.3, 14.1, 11.8.

ESI-MS: calculated for C$_{26}$H$_{40}$BrN$_5$O$_2$ 533.2365; found m/z = 556.2205 [M+Na]$^+$.

4.1.36. N-butyl-2-(N-(2-hydroxyethyl)-2-(4-(m-tolyl)-1H-1,2,3-triazol-1-yl)acetamido)-2-(4-(trifluoromethyl)phenyl)acetamide - Compound 9

Compound **9** was obtained by following the general procedure (**C**), from the reaction between **II (b,c,h)** and 1-ethynyl-3-methylbenzene (**l**), as a yellowish oil (10.4 mg, 78 % yield after HPLC purification).

RP-HPLC t_R = 27.1 min, gradient condition: from 5 % B ending to 100 % B 40 min, flow rate of 4 mL/min, λ = 240 nm.

1H NMR (400 MHz, CD$_3$OD): δ 8.29 (s, 1H), 7.76 (d, J = 8.1 Hz, 2H), 7.69 (s, 1H), 7.64 (d, J = 8.1 Hz, 3H), 7.34 (t, J = 7.7 Hz, 1H), 7.20 (d, J = 7.7 Hz, 1H), 5.84–5.69 (m, 2H), 3.68–3.59 (m, 1H), 3.57–3.43 (m, 3H), 3.33–3.17 (m, 2H), 2.42 (s, 3H), 1.53–1.44 (m, 2H), 1.38–1.27 (m, 3H), 0.91 (t, J = 7.3 Hz, 3H).

13C NMR (101 MHz, CD$_3$OD): δ 169.9, 168.2, 147.5, 139.1, 138.3, 130.4 3C, 130.2 (2C), 128.6, 128.4 (2C), 125.9 (2C), 125.3, 122.6, 122.4, 62.8, 59.5, 51.4 (2C), 39.1, 30.8, 20.1, 19.6, 12.6.

ESI-MS: calculated for $C_{26}H_{30}F_3N_5O_3$ 517.2301; found m/z = 518.2407 [M + H]$^+$.

4.1.37. N-butyl-2-(N-propyl-2-(4-(m-tolyl)-1H-1,2,3-triazol-1-yl)acetamido)-2-(4-(trifluoromethyl)phenyl)acetamide - Compound 10

Compound **10** was obtained by following the general procedure (**C**), from the reaction between **II (b,c, i)** and 1-ethynyl-3-methylbenzene (**l**), as a white powder (116.3 mg, 68 % yield after HPLC purification).

RP-HPLC t_R = 28 min, gradient condition: from 5 % B ending to 100 % B 40 min, flow rate of 4 mL/min, λ = 240 nm.

1H NMR (400 MHz, CDCl$_3$): δ 8.00 (s, 1H), 7.69–7.58 (m, 4H), 7.52 (d, J = 8.4 Hz, 2H), 7.32 (t, J = 7.7 Hz, 1H), 7.15 (d, J = 7.6, 1H), 5.75 (s, 1H), 5.35 (s, 2H), 3.43–3.35 (m, 2H), 3.30–3.21 (m, 2H), 2.40 (s, 3H), 1.63–1.53 (m, 1H), 1.49–1.40 (m, 2H), 1.34–1.17 (m, 3H), 0.88 (t, J = 7.3 Hz, 3H), 0.78 (t, J = 7.3 Hz, 3H).

13C NMR (101 MHz, CDCl$_3$): δ 168.3, 166.2, 138.3 (2C), 131.6, 131.3, 131.0, 130.2, 129.6, 129.0, 128.7, 126.5 (2C), 125.9, 122.9 (2C), 121.6, 63.2, 51.1, 49.1, 39.6, 31.4, 23.2, 21.4, 20.0, 13.6, 11.1.

ESI-MS: calculated for $C_{27}H_{32}F_3N_5O_2$ 515.2508; found m/z = 538.2368 [M + Na]$^+$.

4.1.38. N-butyl-2-(6-chloropyridin-3-yl)-2-(2-(4-(1-(4-fluorophenyl)-1-hydroxyethyl)-1H-1,2,3-triazol-1-yl)-N-(2-methylbutyl)acetamido)acetamide - Compound 11

Compound **11** was obtained by following the general procedure (**C**), from the reaction between **II (c,g,m)** and 2-(4-fluorophenyl)but-3-yn-2-ol (**t**), as a white powder (145.6 mg, 72 % yield after HPLC purification).

RP-HPLC t_R = 27 min, gradient condition: from 5 % B ending to 100 % B 40 min, flow rate of 4 mL/min, λ = 240 nm.

1H NMR (400 MHz, CDCl$_3$): δ 8.30 (t, J = 2.9 Hz, 1H), 7.85–7.75 (m, 1H), 7.55 (s, 1H), 7.47–7.41 (m, 2H), 7.34 (d, J = 8.2 Hz, 1H). 7.07–6.96 (m, 2H), 6.19 (s, 1H), 5.30–5.20 (m, 2H), 3.49 (s, 3H), 3.34–3.26 (m, 2H), 3.24–3.17 (m, 2H), 1.95 (s, 2H), 1.44–1.36 (m, 3H), 1.28–1.20 (m, 3H), 0.94–0.91 (m, 1H), 0.87–0.80 (t, J = 7.3 Hz, 9H).

13C NMR (101 MHz, CDCl$_3$): δ 167.7, 166.6, 163.3, 160.7, 151.9, 150.1, 141.9, 137.5, 129.7, 129.4, 127.2, 124.5, 123.4, 115.0, 115.5, 114.8, 63.6, 54.7, 51.2, 50.7, 39.8, 34.2, 31.3, 26.9, 20.3, 16.6, 13.4, 11.5.

ESI-MS: calculated for $C_{28}H_{36}ClFN_6O_3$ 558.2521; found m/z = 581.2392 [M + Na]$^+$.

4.1.39. N-butyl-2-(2,6-dichloropyridin-3-yl)-2-(2-(4-(1-(4-fluorophenyl)-1-hydroxyethyl)-1H-1,2,3-triazol-1-yl)-N-(2-methylbutyl)acetamido)acetamide - Compound 12

Compound **12** was obtained by following the general procedure (**C**), from the reaction between **II (c,g,n)** and 2-(4-fluorophenyl)but-3-yn-2-ol (**t**), as a white powder (48 mg, 58 % yield after HPLC purification).

RP-HPLC t_R = 28 min, gradient condition: from 5 % B ending to 100 % B 40 min, flow rate of 4 mL/min, λ = 240 nm.

1H NMR (400 MHz, CDCl$_3$): δ 8.03 (t, J = 2.9 Hz, 1H), 7.57 (s, 1H), 7.47–7.41 (m, 2H), 7.33 (d, J = 8.2 Hz, 1H), 7.02 (t, J = 8.8 Hz, 2H), 5.97 (s, 1H), 5.55 (d, J = 8.4 Hz, 1H), 5.00–4.89 (m, 2H), 3.29–3.21 (m, 3H), 3.15–3.05 (m, 2H), 1.96 (s, 3H), 1.49–1.38 (m, 3H), 1.33–1.21 (m, 3H), 1.10–1.01 (m, 1H), 0.92–0.77 (m, 9H).

13C NMR (101 MHz, CDCl$_3$): δ 167.5, 166.8, 164.2, 161.7, 161.3, 151.4, 151.1, 142.2, 137.2, 129.5, 128.2, 127.2, 123.8, 116.2, 115.5, 115.2, 62.2, 58.7, 55.2, 51.4, 40.0, 34.6, 31.2, 26.9, 20.1, 16.9, 13.7, 11.4.

ESI-MS: calculated for $C_{28}H_{36}Cl_2FN_6O_3$ 592.2132; found m/z = 615.1994 [M + Na]$^+$.

4.1.40. 2-(4-Bromo-2-chloropyridin-3-yl)-N-butyl-2-(2-(4-(3-hydroxyphenyl)-1H-1,2,3-triazol-1-yl)-N-(2-methylbutyl)acetamido)acetamide - Compound 13

Compound **13** was obtained by following the general procedure (**C**), from the reaction between **II (c,g,o)** and 3-ethynylphenol (**u**), as a white powder (39.6 mg, 47 % yield after HPLC purification).

RP-HPLC t_R = 26 min, gradient condition: from 5 % B ending to 100 % B 40 min, flow rate of 4 mL/min, λ = 240 nm.

1H NMR (400 MHz, CDCl$_3$): δ 8.35 (d, J = 5.2 Hz, 1H), 8.24 (d, J = 5.2 Hz, 1H), 7.95 (s, 1H), 7.61 (d, J = 5.2 Hz, 1H), 7.41–7.27 (m, 4H), 6.83 (dd, J = 7.3, J = 3.6, 1H), 6.02–5.89 (m, 1H), 5.45–5.33 (m, 2H), 3.56–3.40 (m, 2H), 3.37–3.21 (m, 2H), 1.53–1.45 (m, 3H), 1.38–1.23 (m, 3H), 0.93–0.84 (m, 6H), 0.81–0.73 (m, 3H).

13C NMR (101 MHz, CDCl$_3$): δ 167.2, 166.8, 156.6 (2C), 149.7, 147.2, 140.1, 130.8, 130.0, 128.6, 125.4, 122.7, 117.9, 115.9, 112.9, 35.7, 17.4, 16.6, 13.6, 11.3, 51.4, 40.5, 30.9, 27.3, 26.8, 20.5.

ESI-MS: calculated for $C_{26}H_{32}BrClN_6O_3$ 590.1408; found m/z = 613.1281 [M + Na]$^+$.

4.1.41. 2-(2-Bromo-5-hydroxyphenyl)-N-butyl-2-(2-(4-(3-methoxyphenyl)-1H-1,2,3-triazol-1-yl)-N-(2-methylbutyl)acetamido)acetamide - Compound 14

Compound **14** was obtained by following the general procedure (**C**), from the reaction between **II (c,g,p)** and 1-ethynyl-3-methoxybenzene (**v**), as a yellowish powder (60.7 mg, 74 % yield after HPLC purification).

RP-HPLC t_R = 30.2 min, gradient condition: from 5 % B ending to 100 % B 40 min, flow rate of 4 mL/min, λ = 240 nm.

1H NMR (400 MHz, CDCl$_3$), mixture of rotamers: δ 8.00 (s, 1H), 7.22–7.14 (m, 3H), 6.94 (d, J = 2.9 Hz, 1H), 6.88–6.82 (m, 1H), 6.51 (dd, J = 8.9, 3.8 Hz, 1H), 6.02–5.95 (m, 1H), 5.50–5.32 (m, 2H), 5.27–5.19 (m, 1H), 3.84 (s, 3H), 3.42–3.30 (m, 2H), 3.27–3.21 (m, 1H), 3.12–3.02 (m, 1H), 1.72 (s, 1H), 1.48–1.39 (m, 1H), 1.37–1.27 (m, 2H), 1.26–1.15 (m, 3H), 1.14–1.10 (m, 2H), 0.99–0.85 (m, 4H), 0.76 (t, J = 7.3, 3H).

13C NMR (101 MHz, CDCl$_3$), mixture of rotamers: δ 167.6, 166.6, 164.1, 150.8, 145.4, 142.4, 135.6, 133.6, 131.9, 131.7, 129.1, 127.4, 124.6, 107.8, 56.3, 52.8, 51.2, 38.7, 34.1, 30.8, 26.3, 20.6, 19.5, 18.9 (2C), 16.5, 13.5, 11.4.

ESI-MS: calculated for $C_{28}H_{36}BrN_5O_4$ 585.1951; found m/z = 608.1812 [M + Na]$^+$.

4.1.42. N-butyl-2-(2-(4-(2,5-dimethylphenyl)-1H-1,2,3-triazol-1-yl)-N-(2-methylbutyl)acetamido)-2-(1H-indazol-6-yl)acetamide - Compound 15

Compound **15** was obtained by following the general procedure (**C**), from the reaction between **II (c,g,q)** and 2-ethynyl-1,4-dimethylbenzene (**w**), as a green powder (98 mg, 49 % yield after HPLC purification).

RP-HPLC t_R = 28.2 min, gradient condition: from 5 % B ending to 100 % B 40 min, flow rate of 4 mL/min, λ = 240 nm.

1H NMR (400 MHz, CDCl$_3$), mixture of rotamers: δ 7.91 (s, 1H), 7.75 (d, J = 8.5 Hz, 1H), 7.61 (d, J = 7.3 Hz, 1H), 7.53 (s, 1H), 7.18–7.04 (m, 4H), 5.66–5.55 (m, 1H), 5.35–5.23 (m, 2H), 3.41–3.35 (m, 1H), 3.33–3.20 (m, 2H), 2.39 (s, 3H), 2.33 (s, 3H), 1.42–1.33 (m, 2H), 1.27–1.16 (m, 3H), 0.99 (d, J = 6.4 Hz, 1H), 0.89–0.78 (m, 9H), 0.76 (t, J = 7.3 Hz, 2H).

13C NMR (101 MHz, CDCl$_3$), mixture of rotamers: δ 168.8, 166.7,

135.5 (3C), 132.3 (2C), 130.7 (3C), 129.4 (2C), 129.2, 129.1 (2C), 125.7, 124.1, 67.3, 55.3, 51.5, 39.7, 34.2, 31.1, 27.0, 20.8, 20.7, 19.9, 16.9, 13.6, 11.2.

ESI-MS: calculated for $C_{30}H_{39}N_7O_2$ 529.3165; found m/z = 552.3015 $[M + Na]^+$.

4.1.43. N-butyl-2-(2,4-dioxo-1,2,3,4-tetrahydropyrimidin-5-yl)-2-(N-(2-methylbutyl)-2-(4-(2,4,5-trimethylphenyl)-1H-1,2,3-triazol-1-yl) acetamido)acetamide - Compound 16

Compound **16** was obtained by following the general procedure (**C**), from the reaction between **II (c,g,r)** and 1-ethynyl-2,4,5-trimethylbenzene (**x**), as yellowish powder (327.3 mg, 51 % yield after HPLC purification).

RP-HPLC t_R = 25.8 min, gradient condition: from 5 % B ending to 100 % B 40 min, flow rate of 4 mL/min, λ = 240 nm.

^{1}H NMR (400 MHz, CD₃OD), mixture of rotamers: δ 8.06 (s, 1H), 7.66 (s, 1H), 7.43 (s, 1H), 7.05 (s, 1H), 5.52 (dd, J = 16, 7.6 Hz, 2H), 5.23 (d, J = 16 Hz, 1H), 3.46–3.32 (m, 2H), 3.21–3.11 (m, 2H), 2.35 (s, 3H), 2.26 (s, 6H), 1.80–1.67 (m, 1H), 1.48–1.39 (m, 2H), 1.33–1.28 (m, 2H), 1.07–1.01 (m, 2H), 1.02–0.84 (m, 9H).

^{13}C NMR (101 MHz, (CD₃)₂SO), mixture of rotamers: δ 167.6, 166.6, 164.1, 150.8, 145.4, 142.4, 135.6, 133.6, 131.9, 131.7, 129.1, 127.4, 124.6, 107.8, 56.3, 52.8, 51.2, 38.7, 34.1, 30.8, 26.3, 20.6, 19.5, 18.9 (2C), 16.5, 13.5, 11.4.

ESI-MS: calculated for $C_{28}H_{39}N_7O_4$ 537.3064; found m/z = 560.2924 $[M + Na]^+$.

4.2. Computational details

4.2.1. Preparation and molecular docking of the reference compound 7

Compound **7** was drawn with 2D sketcher of Maestro (**Schrödinger Release 2021-1**: Maestro, Schrödinger, LLC, New York, NY, 2021) in the Schrödinger Suite and then prepared using LigPrep (**Schrödinger Release 2021-1**: LigPrep, Schrödinger, LLC, New York, NY, 2021) module accounting the protonation state at a pH = 7.4 ± 1.0 and minimizing the structure with OPLS 2005 force field. Prior to perform docking calculations, the Protein Preparation Wizard workflow (**Schrödinger Release 2021-1**: Protein Preparation Wizard, Epik, Schrödinger, LLC, New York, NY, 2021; Impact, Schrödinger, LLC, New York, NY; Prime, Schrödinger, LLC, New York, NY, 2021) was employed using the crystal structure of the murine BAG domain of Bcl2-associated athanogene 3 (PDB: 1UK5), given the absence of human crystallized structures on the Protein Data Bank. All hydrogen atoms were added, bond orders were assigned, and all water molecules were removed. The grid used for all calculations was built considering the entire structure of the protein, due to the absence of previous information related to a BAG3 modulator (innerbox dimensions of 40 Å and outerbox dimensions of 46 Å with center coordinates in Å: X = 0.0; Y = −8.0; Z = 3.0). Docking calculations were performed using the prepared structure in Glide software (**Schrödinger Release 2021-1**: Glide, Schrödinger, LLC, New York, NY, 2021) at standard precision (SP) level using Ligand docking panel in Schrödinger Suite (generating a maximum of 50 output poses).

4.2.2. Generation of the virtual library

The 1,2,3–triazole chemical core was prepared using LigPrep module accounting the protonation state at a pH = 7.4 ± 1.0 and minimizing the structure with OPLS 2005 force field. Employing CombiGlide software (**Schrödinger Release 2021-1**: CombiGlide, Schrödinger, LLC, New York, NY, 2021), a virtual library of 85,680 1,2,3-triazole-based compounds was generated: 714 aromatic aldehydes and 120 terminal alkynes (filtered considering a molecular weight less than 250 g/mol) were considered according to the specific synthetic route (Fig. 1) and commercial availability of synthons (Merck). In particular, for the library construction, driven by the results of compound **7**, the isocyanide and amine moieties remained unchanged. On the produced virtual

library, pharmacokinetic properties were computed using Qikprop software (**Schrödinger Release 2021-1**: Qikprop, Schrodinger, LLC, New York, NY, USA, 2021) included in the Schrödinger Suite. Thereafter, the library was filtered using the Ligand Filtering utilities implemented in Schrödinger Suite and following the Lipinski filter in order to obtain the final 17,390 compounds that were selected for the subsequent molecular docking calculations. Specifically, the following parameters were accounted: (a) molecular weight ≤700 g/mol; (b) #stars: number of property or descriptor values that fall outside the 95 % range of similar values for known drugs (range or recommended values: 0–5); (c) rtvFG: number of reactive functional groups, which can lead to false positive in high-throughput screening (HTS) assays and to decomposition, reactivity, or toxicity problems *in vivo* (range or recommended values: 0–2); (d) #donorHB: estimated number of hydrogen bonds that would be donated (recommended values: 0–5); (e)#accptHB: estimated number of hydrogen bonds that would be accepted by the solute from water molecules in an aqueous solution by the solute to water molecules in an aqueous solution (recommended values: 0–10); (f) #QPlogPo/w: predicted octanol/water partition coefficient (recommended values: 2.0–5.0). After this filtering step, a fast "shape screening" alignment was performed using the Shape Screening panel (**Schrödinger Release 2021-1**: Phase, Schrödinger, LLC, New York, NY, 2021) of the Phase software (**Schrödinger Release 2021-1**: Phase, Schrödinger, LLC, New York, NY, 2021) and considering the 3D structure of the promising compound **7**. In particular, for the screened compounds, the sampling was performed allowing the conformers around the amide bond to vary freely, and 100 maximum number of conformers were considered for the shape computation. Then, a ranking from the best to worst values was obtained and only those compounds with a shape similarity higher than 0.700 were saved.

4.2.3. Molecular docking of the generated library on BAG3

The filtered library (8184 compounds) was then used as input for the molecular docking calculations against BAG-binding domain of BAG3 protein, using the protein grid previously mentioned. The ligand docking was performed using the Standard Precision scoring and sampling docking (SP) (Ligand docking panel in Schrödinger Suite) and generating a maximum of 50 output poses for each compound in order to perform and exhaustive sampling of all possible conformations in the binding site of BAG3. The selected compounds were ranked considering the best docking score and visually inspected in order to select those featuring the promising predicted binding with the target protein and able to establish interactions with fundamental amino acids.

4.2.4. Molecular docking of compound 16 on HSP70

Starting from the results obtained from LiP experiments, molecular docking of compound **16** on HSP70 was carried out. The Protein Preparation Wizard workflow (Maestro, Schrodinger) was employed using the crystal structure of the HSP70 (PDB: 5AQX). All hydrogen atoms were added, bond orders were assigned, and all water molecules and the crystallized ligand were removed. Two grids were generated considering the specific amino acid sequences of tryptic peptides as a centroid: in detail, for I-[172–187]-R peptide, a grid was generated featuring innerbox dimensions of 10 Å and outerbox dimensions of 26 Å (center coordinates in Å: X = −24.33; Y = −7.98; Z = 5.00); while for F-[302–311]-R peptide, a grid was generated featuring innerbox dimensions of 10 Å and outerbox dimensions of 23 Å (center coordinates in Å: X = −19.66; Y = 0.123; Z = −22.31). Docking calculations were performed at extra precision (XP) level implemented in Glide software, saving 20 poses for the ligand in order to perform an exhaustive sampling of all possible conformations in the binding sites.

4.2.5. Molecular dynamics simulation

Simulations were carried out for the poses selected from docking with the Desmond software (version 7.6). Specifically, the starting systems were prepared accounting the TIP3P water model for solvatation

and OPLS-2005 force field and ensemble as NPT. For BAG3, Na^+ was added to neutralize the system and a cubic box with a 10 Å buffer distance was set; for HSP70, Cl^- was added and the same cubic box was set. The pressure and temperature were kept constant at 1 bar and 310 K. A minimization step of 6250 ps (NVT) and an equilibration step of 750 ps (NVT) and 3000 ps (NPT) were performed. After, MD simulations in NPT were carried out over a time frame of 1000 ns (**Schrödinger Release 2024-4**: Desmond Molecular Dynamics System, D. E. Shaw Research, New York, NY, 2024. Maestro-Desmond Interoperability Tools, Schrödinger, New York, NY, 2024).

4.3. SPR assay

Recombinant human BAG3 protein (Bcl2-associated athanogene 3) was purchased from Novus Biologicals (Littleton, Colorado) while the BAG3 domain (BAG3-BD) was obtained from ARETA International S.r.l. (Gerenzano, Italy). The BAG3 inhibitor used in our study was (Z)-ethyl 2-(5-(3,4-dihydroxybenzylidene)-2,4-dioxothiazolidin-3-yl)acetate (**LK4**), a compound previously identified by our group [24]. Recombinant human HSP70 protein (Heat shock protein 70) was sourced from Enzo Life Sciences (Farmingdale, New York, USA). HSP70 inhibitor, **YM-01**, (2-((Z)-((E)-3-ethyl-5-(3-methylbenzo[d]thiazol-2(3H)-ylidene)-4-oxothiazolidin-2-ylidene)methyl)-1-methylpyridin-1-ium chloride) was obtained from Merck (Darmstadt, Germany) [28]. Surface Plasmon Resonance Spectroscopy (SPR) analyses were conducted to evaluate the binding affinities of the synthesized compounds against BAG3, BAG-BD, and HSP70 proteins using a Biacore T200 optical biosensor equipped with research-grade CM5 sensor chips (Cytiva, Marlborough, USA). BAG3, BAG-BD, and HSP70 proteins were immobilized on the CM5 sensor chip surface following standard amine-coupling protocols. Specifically, BAG3 protein (0.067 µg µl^{-1} in 10 mM CH_3COONa, pH 4.5) was immobilized at a flow rate of 10 µL min^{-1}, achieving a density of 14 kRU. The BAG domain (0.38 µg µl^{-1} in 10 mM CH_3COONa, pH 4.5) was immobilized under similar conditions, resulting in a density of 4 kRU. HSP70 (0.045 µg µl^{-1} in 10 mM CH3COONa, pH 4.5) was also immobilized at a flow rate of 10 µL min^{-1}, achieving a density of 20 kRU. For the experiments, surfaces of BAG3, BAG-BD, and HSP70, along with an unmodified reference surface, were prepared for simultaneous analyses. Compounds **1**–**16**, **LK4,** and **YM-01** were dissolved to prepare 10 mM solutions in 100 % DMSO, then diluted 1:20 (v/v) in PBS-P (PBS–P buffer: 0.2 M phosphate buffer, 27 mM KCl, 1.37 M NaCl, 0.5 % surfactant P20) to achieve a final DMSO concentration of 5.0 %. The compounds were injected in a series of concentrations (1:2 dilution, 10 different concentrations), spanning from 0 to 100 µM. The concentration series were prepared in 96-well plates. SPR experiments were conducted at 25 °C, with a flow rate of 20 µL min^{-1}, allowing for 90 s of association monitoring and 400 s of dissociation monitoring. Changes in mass, reflective of the binding response, were recorded as resonance units (RU). K_D values were determined using the Biaevaluation software performing a global fit of the double-referenced association and dissociation data to a 1:1 interaction model (**See** Supporting Information, Figs. S86–S99) [25].

4.4. Building MRM methods

To develop methods for the mass analysis, the HSP70 and BAG3 tryptic peptides were first identified in the PeptideAtlas data repository according to their specific accession number (P0DMV8 and O95817 respectively) and then analyzed using the Human build of SRMAtlas, which provided the mass-to-charge (m/z) values of the possible fragments for each peptide (Query parameters as follows: number of highest intensity fragment ions to keep: 8; target instrument: QTRAP 5500; transitions source: QTOF, Agilent QQQ, Qtrap5500, Ion Trap, Predicted; allowed ions types: b-ions and y-ions; allowed peptides modification: carbamidomethylation of cysteines (C[160])).

The top three optimal transitions for each peptide were chosen to construct MRM preliminary methods, which were subsequently tested using a tryptic-digested HeLa protein extract, obtained as follows: HeLa cells were resuspended in PBS 0.1 % v/v Igepal (137 mM NaCl, 2.7 mM KCl, 10 mM Na_2HPO_4, 2 mM KH_2PO_4, pH 7.4, 0.1 % v/v Igepal) with protease inhibitor solution (GeneSpin). Lysis was achieved using a Dounce homogenizer at 4 °C. The resulting suspension was then centrifuged at 10,000×g for 5 min at 4 °C, and the supernatant was collected and submitted to Bradford assay to estimate protein concentration (BioRad Laboratories, Hercules, CA).

Extensive tryptic digestion was performed by applying an in-solution digestion protocol [52,53]. In brief, proteins were first denatured with urea 4 M/50 mM AmBic and then disulfide bonds were reduced with 10 mM DTT for 1 h at 25 °C (500 rpm, thermomixer, Biosan), and free thiols were alkylated with 20 mM iodoacetamide (500 rpm, 30 min at 25 °C in the dark). Subsequently, 10 mM DTT was introduced again (10 min, 25 °C, 500 rpm) to quench the excess of iodoacetamide. Urea concentration was diluted to 1 M with 50 mM AmBic, and a trypsin/LysC solution (enzyme to proteins ratio of 1:100 w/w, Promega, Madison, Wisconsin) was added at 37 °C with shaking overnight. Digestion was stopped lowering the solution pH to 3 with formic acid (FA), and the peptides were initially dried under vacuum and re-dissolved in 1 mL 5 % FA for the subsequent desalting step using a Sep-Pak C18 1 cc (50 mg) cartridge (Waters, Milford, MA, USA).

The desalted mixtures were again dried under vacuum and resuspended in 10 % FA (2 µg/µL final concentration) for the mass analysis.

The chromatographic separation was achieved by injecting 15 µL of each sample and using a Kinetex PS C18 column (50 × 2.1 mm, 2.6 µm, 100 Å, Phenomenex, Torrance, USA) for the separation with a linear gradient from 5 % to 95 % of B in 20 min (A: 0.1 % FA in H_2O, B: 0.1 % FA in CH_3CN). The eluted peptides were detected using Multiple Reaction Monitoring (MRM) in positive ion mode on the 6500 Q-Trap (mass parameters as follows: curtain gas (CUR) = 30; Ion-Spray voltage (IS) = 5500; temperature (TEM) = 250 °C; ion source gas 1 (GS1) = 25; ion source gas 2 (GS2) = 25; Declustering Potential (DP) = 80, Entrance Potential (EP) = 15, Collision Energy (CE) = 35, Collision Cell Exit Potential (CXP) = 12, dwell time for each peptide was 80 ms. Data acquisition and processing were performed using Analyst software 1.6.2 (ABSciex, Foster City, CA, USA).

4.4.1. t-LiP experiment

HeLa cell lysate, obtained as previously described, was incubated with compound **16** (100 µM) and with DMSO for 1h at room temperature under shaking (Mini-Rotator, Biosan) and then treated with subtilisin (enzyme to proteins ratio of 1:1500 w/w) for 30 min at 25 °C under shaking (500 rpm, Thermomixer, Biosan), leaving an undigested sample (with no molecule) as control. The enzyme was then quenched with PMSF (1 mM final concentration), and samples were submitted to the in-solution tryptic digestion protocol previously described. Thus, mass analysis of the t-LiP samples was performed using the earlier optimized MRM method (*see above*). Analyst Software (AB Sciex) was used to measure the areas of each tryptic peptide peak. Fold Changes were calculated for each peptide as follows: Peak Area $_{sample\ with\ 16}$/Peak Area $_{reference\ sample}$ and considered relevant when higher than 1.5.

4.5. Cell culture

Cell lines of human cervical carcinoma (HeLa), human malignant melanoma (A375), human lung adenocarcinoma (A549), and immortalized human keratinocyte (HaCaT) were cultured in DMEM/high glucose supplemented with FBS (10 %, v/v), 2 mM/L glutamine, penicillin (100 U/mL), and streptomycin (100 mg/mL) at 37 °C in a humidified atmosphere with 5 % CO_2. Subculturing every 2 days was performed to ensure logarithmic growth. The cell lines were kindly donated by Prof Ornella Moltedo, Department of Pharmacy University of Salerno.

4.5.1. Cell viability

Cell viability was determined by measuring mitochondrial metabolic activity using a colorimetric assay based on the reduction of 3-[4,5-dimethylthiazol-2,5-diphenyl-2H-tetrazolium bromide (MTT) to purple formazan. Stock solutions of compounds **7**, **15**, **16**, and **YM-01** (50 mM in DMSO) were stored at −20 °C in the dark and diluted just before addition to the sterile culture medium [24,28]. Briefly, HeLa ($3.5x10^3$ cells/well), A375 ($5x10^3$ cells/well), A549 ($3.5x10^3$ cells/well), and Hacat ($5.0x10^3$ cells/well) were seeded in triplicate in 96-well plates. After 24 h of growth to allow attachment to the wells, the cells were incubated with tested compounds at various concentrations (10 and 50 μM), DMSO 0.1 % (v/v) (Ctrl neg), and DMSO 10 % (v/v) (Ctrl pos) for 72 h. After treatment, 20 μL of MTT (5 mg/mL in PBS) was added, and the cells were incubated for an additional 3h at 37 °C. The formazan crystals were then dissolved in 100 μL of a buffer containing 50 % (v/v) N, N-dimethylformamide, and 20 % SDS (pH 4.5). Absorbance was measured at 570 nm using a Multiskan™ GO Microplate Spectrophotometer (Thermo Fisher Scientific, Waltham, Massachusetts, USA) [25]. Only for compound **7**, the assays were performed on all three tumor cell lines. The assays for the other molecules were performed only on HeLa, as representatives of tumor cells, and on Hacat, as representatives of healthy cells. For compounds **16** and **YM-01**, which exhibited a relevant antiproliferative activity on HeLa and no effect on HaCaT, the proliferation assays were also performed at seven different concentrations (ranging from 1.56 μM to 100 μM) to determine the IC_{50} value after 72 h. The IC_{50} values, representing the concentration resulting in 50 % inhibition of cell survival, were calculated and compared to control cells treated with DMSO using GraphPad Prism8.0 software by nonlinear regression of dose-response inhibition.

4.5.2. Cell cycle analysis

Hypodiploid nuclei were analyzed using PI staining by flow cytometry. HeLa cells ($1x10^5$ cells/well) were grown in 12-well plates and allowed to adhere for 24 h. Afterward, the medium was replaced with fresh medium, and cells were treated with compound **16** (10, 25, and 50 μM), **YM-01** (1, 5, and 10 μM), DMSO 0.1 % (v/v) (Ctrl neg), DMSO 10 % (v/v) (Ctrl pos) for 72h. Following treatment, the culture medium was replaced, cells were washed twice with PBS, and then suspended in 500 mL of a solution containing 50 mg/L PI, 0.1 % (w/v) sodium citrate, and 0.1% Triton X-100. Culture medium and PBS were centrifuged, and cell pellets were pooled with cell suspension to retain both dead and living cells for analysis. After incubation at 4 °C for 30 min in the dark, cell nuclei were analyzed with a Becton Dickinson FACSc (Franklin Lakes, New Jersey, USA) a flow cytometer using the Cell Quest program, and the DNA content of the nuclei was registered. Cellular debris was excluded from the analysis by raising the forward scatter threshold, then the percentage of cells in the hypodiploid region (sub-G_0/G_1) was calculated (**See** Supporting Information, Figure S100) [25,28].

4.5.3. Annexin V-FITC/PI staining

The evaluation of apoptosis was assessed using the Annexin V-FITC/PI reagents (Dead Cell Apoptosis Kits with Annexin V for Flow Cytometry, Thermo Fisher Scientific, Waltham, Massachusetts, USA). HeLa cells (2×10^4) were seeded into 24-well plates and incubated for 72 h with compound **16**. After treatment, the collected cells were resuspended in a 100 μL assay buffer, then 5 μL Annexin V-FITC and 1 μL PI reagents were added following an incubation for 15 min at RT according to the manufacturer's protocol. Cells were analyzed with a Becton Dickinson FACScan flow cytometer using the Cell Quest software, version 4 (Franklin Lakes, New Jersey, USA) [27].

4.5.4. Measurement of caspase 3, caspase 9, and p21 levels

HeLa cells were seeded into 6-well plates ($2.5x10^5$ cells/well) and after 24 h were treated with **16** (10, 25 and 50 μM), **YM-01** (10 μM), or DMSO 0.1 % (Ctrl) for 72 h to assess caspase 3, caspase 9, and p21 levels. Cells were collected, washed with PBS, and incubated at 4 °C first with fixing buffer (containing 1 % formaldehyde, 1 % FBS in PBS) for 20 min and then permeabilized with fix perm solution (fixing buffer containing 0.1 % Triton X100) for 30 min. Afterward, anti-caspase 3 (1:500; SC-7272, Santa Cruz, California, USA), anti-caspase 9 (1:50; BS-0049R, Bioss Antibodies, Woburn, USA), or anti-p21 (1:400; MA5-31479, Thermo Fisher Scientific, Waltham, USA) antibodies were added for 30 min at 4 °C. Subsequently, cells were incubated with anti-mouse (1:50; A90-116D3, Bethyl, Montgomery, USA) or anti-rabbit (A120-101D2, Bethyl, Montgomery, USA) secondary antibodies for 30 min at 4 °C. Cell fluorescence was evaluated using a fluorescence-activated cell sorter (FACSscan, Becton Dickinson, Franklin Lakes, New Jersey, USA) and analyzed with the Cell Quest software (4.0, Becton Dickinson, North Ryde, Australia). Data were shown as a percentage of positive cells (**YM-01** activity) (**See** Supporting Information, Figures S101 – S103) [25,28].

4.5.5. Measurement of FOXM1 levels through Western blot analysis

The HeLa cell line was seeded in 60 mm culture dishes (20×104) and treated with compound **16** (30, 15 μM) for 72 h. After treatments, the cells were washed twice, detached with a scraper, and centrifuged for 10 min (400 g, 4 °C) to remove debris. Total proteins were extracted by lysis buffer (20 mM Tris-HCl pH 7.5, 150 mM NaCl, 1 mM Na_2EDTA, 1 mM EGTA, 2 % NP-40, 1 % sodium deoxycholate, 1x protease, and phosphatase inhibitor cocktail) for 30 min. Cell lysates were then centrifuged at 18,800 g for 15 min at 4 °C. Protein concentration was determined by the Bradford assay using bovine serum albumin as standard. 30 μg of total proteins were run on 10 % SDS-PAGE and transferred to nitrocellulose membranes using a minigel apparatus (Bio-Rad Laboratories, Richmond, Canada). Ponceau S dye is applied to stain the proteins on the membrane a red color, after which the membrane is rinsed with MQ water to remove excess stain. Blots were blocked in phosphate buffered saline, containing Tween-20 0.1 % and 10 % nonfat dry milk for 2 h at room temperature and incubated overnight with specific primary antibodies at 4 °C with slight agitation. Mouse monoclonal anti-FOXM1 (1:500, Invitrogen) was used. Mouse monoclonal anti-β-Tubulin (1:1000, Sigma Aldrich) was used as loading control. After washes in PBS/Tween-20 0.1 % the anti-mouse (1:5000, Pierce, Thermo Fisher Scientific) peroxidase-linked secondary antibody was added for 1 h at room temperature. Enhanced chemiluminescence and the LAS 4000 system (GE Healthcare, Chicago, IL, USA) were used to detect antigen–antibody complexes. A densitometry analysis of the autoradiographs was performed by using the ImageJ program, version 1.47 (**See** Supporting Information, Figure S104) [54].

4.6. HSP70 activity

A series of dilutions of the compounds were prepared with 10 % DMSO in assay buffer and 2.5 μl of the dilution was added to a 25 μl reaction so that the final concentration of DMSO is 1 % in all of reactions. After a 30-min pre-incubation step at room temperature including HSP70, HSP40, and the compound, ATP was added to initiate the reactions and they were conducted at 30^oC for 1 h in a 25 μl mixture containing ATP, assay buffer, HSP70, HSP40, and the test compound. After the 1-h reaction, 25 μL of ADP-Glo reagent was added to each well and the reactions were incubated at room temperature for 1 h. After the 1-h incubation with ADP-Glo, 50 μL of detection reagent was added to each well and the reactions were incubated at room temperature for 20 min. Following this incubation, the plates were read [55]. Luminescence was measured using a BioTek Synergy™ 2 microplate reader (BioTek, Winooski, Vermont, USA). HSP70 activity assays were performed in duplicates. The luminescence data were analyzed using the computer software, Graphpad Prism. In the absence of the compound, the luminescence (Lt) in each data set was defined as 100 % activity. In the absence of HSP70, the luminescence (Lb) in each data set was defined as 0 % activity. The percent activity in the presence of each compound was calculated according to the following equation: % activity = [(L - Lb)/(Lt - Lb)] × 100, where L = the luminescence in the presence of the

compound, Lb = the luminescence in the absence of HSP70, and Lt = the luminescence in the absence of the compound. The percentage inhibition was calculated according to the following equation: % inhibition = 100 - % activity.

CRediT authorship contribution statement

Dafne Ruggiero: Writing – original draft, Methodology, Investigation, Formal analysis, Conceptualization. **Emis Ingenito:** Writing – original draft, Investigation, Formal analysis. **Eleonora Boccia:** Writing – original draft, Software, Investigation, Formal analysis. **Vincenzo Vestuto:** Investigation, Formal analysis. **Gilda D'Urso:** Investigation, Formal analysis. **Alessandra Capuano:** Investigation, Formal analysis. **Agostino Casapullo:** Methodology, Conceptualization. **Stefania Terracciano:** Methodology, Conceptualization. **Giuseppe Bifulco:** Software, Resources, Methodology. **Gianluigi Lauro:** Software, Resources, Methodology, Conceptualization. **Ines Bruno:** Writing – original draft, Supervision, Methodology, Investigation, Conceptualization.

Funding

Declaration of competing interest

The authors declare that they have no known competing financial interests or personal relationships that could have appeared to influence the work reported in this paper.

Appendix A. Supplementary data

Supplementary data to this article can be found online at https://doi.org/10.1016/j.ejmech.2025.117358.

Data availability

Data will be made available on request.

References

[1] F.U. Hartl, M. Hayer-Hartl, Molecular chaperones in the cytosol: from nascent chain to folded protein, Science 295 (5561) (2002) 1852–1858.

[2] F.U. Hartl, A. Bracher, M. Hayer-Hartl, Molecular chaperones in protein folding and proteostasis, Nature 475 (7356) (2011) 324–332.

[3] Y.E. Kim, M.S. Hipp, A. Bracher, M. Hayer-Hartl, F. Ulrich Hartl, Molecular chaperone functions in protein folding and proteostasis, Annu. Rev. Biochem. 82 (2013) 323–355.

[4] H. Saibil, Chaperone machines for protein folding, unfolding and disaggregation, Nat. Rev. Mol. Cell Biol. 14 (10) (2013) 630–642.

[5] S. Takayama, J.C. Reed, Molecular chaperone targeting and regulation by BAG family proteins, Nat. Cell Biol. 3 (10) (2001) E237–E241.

[6] M. Kabbage, M.B. Dickman, The BAG proteins: a ubiquitous family of chaperone regulators, Cell. Mol. Life Sci. 65 (2008) 1390–1402.

[7] C. Behl, BAG3 and friends: co-chaperones in selective autophagy during aging and disease, Autophagy 7 (7) (2011) 795–798.

[8] C. Behl, Breaking BAG: the co-chaperone BAG3 in health and disease, Trends in pharmacological sciences 37 (8) (2016) 672–688.

[9] M. Gamerdinger, S. Carra, C. Behl, Emerging roles of molecular chaperones and co-chaperones in selective autophagy: focus on BAG proteins, Journal of molecular medicine 89 (2011) 1175–1182.

[10] A. Rosati, V. Graziano, V. De Laurenzi, M. Pascale, M.C. Turco, BAG3: a multifaceted protein that regulates major cell pathways, Cell Death Dis. 2 (4) (2011) e141-e141.

[11] T. Knezevic, V.D. Myers, J. Gordon, D.G. Tilley, T.E. Sharp, J. Wang, K. Khalili, J. Y. Cheung, A.M. Feldman, BAG3: a new player in the heart failure paradigm, Heart Fail. Rev. 20 (2015) 423–434.

[12] A.P. Bruno, M. Festa, F. Dal Piaz, A. Rosati, M.C. Turco, A. Giuditta, L. Marzullo, Identification of a synaptosome-associated form of BAG3 protein, Cell Cycle 7 (19) (2008) 3104–3105.

[13] A. Paola Bruno, A. Cefaliello, R. D'Auria, A. Crispino, A. Rosati, A. Giuditta, S. Lucia Nori, BAG3 mRNA is present in synaptosomal polysomes of rat brain, Cell Cycle 13 (8) (2014), 1357-1357.

[14] E. Gout, M. Gutkowska, S. Takayama, J.C. Reed, J. Chroboczek, Co-chaperone BAG3 and adenovirus penton base protein partnership, J. Cell. Biochem. 111 (3) (2010) 699–708.

[15] M. Iwasaki, R. Tanaka, A. Hishiya, S. Homma, J.C. Reed, S. Takayama, BAG3 directly associates with guanine nucleotide exchange factor of Rap1, PDZGEF2, and regulates cell adhesion, Biochemical and biophysical research communications 400 (3) (2010) 413–418.

[16] A. Ulbricht, F.J. Eppler, V.E. Tapia, P.F.M. van der Ven, N. Hampe, N. Hersch, P. Vakeel, D. Stadel, A. Haas, P. Saftig, Cellular mechanotransduction relies on tension-induced and chaperone-assisted autophagy, Curr. Biol. 23 (5) (2013) 430–435.

[17] B. Kathage, S. Gehlert, A. Ulbricht, L. Lüdecke, V.E. Tapia, Z. Orfanos, D. Wenzel, W. Bloch, R. Volkmer, B.K. Fleischmann, The cochaperone BAG3 coordinates protein synthesis and autophagy under mechanical strain through spatial regulation of mTORC1, Biochimica et Biophysica Acta (BBA)-Molecular Cell Research 1864 (1) (2017) 62–75.

[18] Q. Liao, F. Ozawa, H. Friess, A. Zimmermann, S. Takayama, J.C. Reed, J. Kleeff, M. W. Büchler, The anti-apoptotic protein BAG-3 is overexpressed in pancreatic cancer and induced by heat stress in pancreatic cancer cell lines, FEBS Lett. 503 (2–3) (2001) 151–157.

[19] S. Homma, M. Iwasaki, G.D. Shelton, E. Engvall, J.C. Reed, S. Takayama, BAG3 deficiency results in fulminant myopathy and early lethality, Am. J. Pathol. 169 (3) (2006) 761–773.

[20] A. Rosati, M. Ammirante, A. Gentilella, A. Basile, M. Festa, M. Pascale, L. Marzullo, M.A. Belisario, A. Tosco, S. Franceschelli, Apoptosis inhibition in cancer cells: a novel molecular pathway that involves BAG3 protein, Int. J. Biochem. Cell Biol. 39 (7–8) (2007) 1337–1342.

[21] A. Gentilella, K. Khalili, BAG3 expression in glioblastoma cells promotes accumulation of ubiquitinated clients in an Hsp70-dependent manner, J. Biol. Chem. 286 (11) (2011) 9205–9215.

[22] V. Felzen, C. Hiebel, I. Koziollek-Drechsler, S. Reißig, U. Wolfrum, D. Kögel, C. Brandts, C. Behl, T. Morawe, Estrogen receptor α regulates non-canonical autophagy that provides stress resistance to neuroblastoma and breast cancer cells and involves BAG3 function, Cell Death Dis. 6 (7) (2015) e1812-e1812.

[23] M.Y. Sherman, V.L. Gabai, Hsp70 in cancer: back to the future, Oncogene 34 (32) (2015) 4153–4161.

[24] S. Terracciano, G. Lauro, A. Russo, M.C. Vaccaro, A. Vassallo, M. De Marco, B. Ranieri, A. Rosati, M.C. Turco, R. Riccio, Discovery and synthesis of the first selective BAG domain modulator of BAG3 as an attractive candidate for the development of a new class of chemotherapeutics, Chemical communications 54 (55) (2018) 7613–7616.

[25] D. Ruggiero, S. Terracciano, G. Lauro, M. Pecoraro, S. Franceschelli, G. Bifulco, I. Bruno, Structural refinement of 2, 4-thiazolidinedione derivatives as new anticancer agents able to modulate the BAG3 protein, Molecules 27 (3) (2022) 665.

[26] F. Budassi, C. Marchioro, M. Canton, A. Favaro, M. Sturlese, C. Urbinati, M. Rusnati, R. Romagnoli, G. Viola, E. Mariotto, Design, synthesis and biological evaluation of novel 2, 4-thiazolidinedione derivatives able to target the human BAG3 protein, Eur. J. Med. Chem. 261 (2023) 115824.

[27] D. Ruggiero, E. Ingenito, E. Boccia, V. Vestuto, M.R. Miranda, S. Terracciano, G. Lauro, G. Bifulco, I. Bruno, Identification of a new promising BAG3 modulator featuring the imidazopyridine scaffold 29 (21) (2024) 5051.

[28] Y. Miyata, X. Li, H.-F. Lee, U.K. Jinwal, S.R. Srinivasan, S.P. Seguin, Z.T. Young, J. L. Brodsky, C.A. Dickey, D. Sun, Synthesis and initial evaluation of YM-08, a blood-brain barrier permeable derivative of the heat shock protein 70 (Hsp70) inhibitor MKT-077, which reduces tau levels, ACS Chem. Neurosci. 4 (6) (2013) 930–939.

[29] X. Li, T. Colvin, J.N. Rauch, D. Acosta-Alvear, M. Kampmann, B. Dunyak, B. Hann, B.T. Aftab, M. Murnane, M. Cho, Validation of the Hsp70–Bag3 protein–protein interaction as a potential therapeutic target in cancer, Mol. Cancer Therapeut. 14 (3) (2015) 642–648.

[30] M.A. Fouad, H. Abdel-Hamid, M.S. Ayoup, Two decades of recent advances of Ugi reactions: synthetic and pharmaceutical applications, RSC advances 10 (70) (2020) 42644–42681.

[31] M. Breugst, H.U. Reissig, The huisgen reaction: milestones of the 1, 3-dipolar cycloaddition, Angew. Chem. Int. Ed. 59 (30) (2020) 12293–12307.

[32] S. Marcaccini, T. Torroba, The use of the Ugi four-component condensation, Nat. Protoc. 2 (3) (2007) 632–639.

[33] M. Meldal, F. Diness, Recent fascinating aspects of the CuAAC click reaction, Trends in Chemistry 2 (6) (2020) 569–584.

[34] P. Pramitha, D. Bahulayan, Stereoselective synthesis of bio-hybrid amphiphiles of coumarin derivatives by Ugi–Mannich triazole randomization using copper catalyzed alkyne azide click chemistry, Bioorg. Med. Chem. Lett 22 (7) (2012) 2598–2603.

[35] G. Chiappetta, A. Basile, A. Barbieri, A. Falco, A. Rosati, M. Festa, R. Pasquinelli, D. Califano, G. Palma, R. Costanzo, The anti-apoptotic BAG3 protein is expressed in lung carcinomas and regulates small cell lung carcinoma (SCLC) tumor growth, Oncotarget 5 (16) (2014) 6846.

[36] R. Franco, G. Scognamiglio, V. Salerno, A. Sebastiani, G. Cennamo, P.A. Ascierto, G. Botti, M.C. Turco, A. Rosati, Expression of the anti-apoptotic protein BAG3 in human melanomas, J. Invest. Dermatol. 132 (1) (2012) 252.

[37] M. De Marco, A. Basile, V. Iorio, M. Festa, A. Falco, B. Ranieri, M. Pascale, G. Sala, P. Remondelli, M. Capunzo, in: Role of BAG3 in Cancer Progression: A Therapeutic Opportunity, Elsevier, 2018, pp. 85–92.

[38] Y. Miyata, X. Li, H.-F. Lee, U.K. Jinwal, S.R. Srinivasan, S.P. Seguin, Z.T. Young, J. L. Brodsky, C.A. Dickey, D.J. Ac. n. Sun, Synthesis and initial evaluation of YM-08, a blood-brain barrier permeable derivative of the heat shock protein 70 (Hsp70) inhibitor MKT-077, which reduces tau levels 4 (6) (2013) 930–939.

[39] Y. Feng, G. De Franceschi, A. Kahraman, M. Soste, A. Melnik, P.J. Boersema, P. P. De Laureto, Y. Nikolaev, A.P. Oliveira, P. Picotti, Global analysis of protein structural changes in complex proteomes, Nat. Biotechnol. 32 (10) (2014) 1036–1044.

[40] A. Fontana, P.P. De Laureto, B. Spolaore, E. Frare, P. Picotti, M. Zambonin, Probing protein structure by limited proteolysis, Acta Biochim. Pol. 51 (2) (2004) 299–321.

[41] P. Picotti, B. Bodenmiller, L.N. Mueller, B. Domon, R. Aebersold, Full dynamic range proteome analysis of S. cerevisiae by targeted proteomics, Cell 138 (4) (2009) 795–806.

[42] R.A. Yost, C.G. Enke, Triple quadrupole mass spectrometry for direct mixture analysis and structure elucidation, Analytical chemistry 51 (12) (1979) 1251–1264.

[43] H.Q. Wang, X. Meng, Y.Y. Gao, B.Q. Liu, X.F. Niu, H.Y. Zhang, Z.X. Du, Characterization of BAG3 cleavage during apoptosis of pancreatic cancer cells, J. Cell. Physiol. 224 (1) (2010) 94–100.

[44] V.M. Virador, B. Davidson, J. Czechowicz, A. Mai, J. Kassis, E.C. Kohn, The anti-apoptotic activity of BAG3 is restricted by caspases and the proteasome, PLoS One 4 (4) (2009) e5136.

[45] T.A. Colvin, V.L. Gabai, J. Gong, S.K. Calderwood, H. Li, S. Gummuluru, O. N. Matchuk, S.G. Smirnova, N.V. Orlova, I.A. Zamulaeva, Hsp70-Bag3 interactions regulate cancer-related signaling networks, Cancer Res. 74 (17) (2014) 4731–4740.

[46] L. Meng, C. Hunt, J.A. Yaglom, V.L. Gabai, M.Y. Sherman, Heat shock protein Hsp72 plays an essential role in Her2-induced mammary tumorigenesis, Oncogene 30 (25) (2011) 2836–2845.

[47] I.C. Wang, Y.-J. Chen, D. Hughes, V. Petrovic, M.L. Major, H.J. Park, Y. Tan, T. Ackerson, R.H. Costa, Forkhead box M1 regulates the transcriptional network of genes essential for mitotic progression and genes encoding the SCF (Skp2-Cks1) ubiquitin ligase, Molecular and cellular biology 25 (24) (2005) 10875–10894.

[48] S.-K. Ko, J. Kim, D.C. Na, S. Park, S.-H. Park, J.Y. Hyun, K.-H. Baek, N.D. Kim, N.-K. Kim, Y.N. Park, A small molecule inhibitor of ATPase activity of HSP70 induces apoptosis and has antitumor activities, Chemistry & biology 22 (3) (2015) 391–403.

[49] M. Pirali, M. Taheri, S. Zarei, M. Majidi, H. Ghafouri, Artesunate, as a HSP70 ATPase activity inhibitor, induces apoptosis in breast cancer cells, Int. J. Biol. Macromol. 164 (2020) 3369–3375.

[50] J. Yang, W. Gong, S. Wu, H. Zhang, S. Perrett, PES inhibits human-inducible Hsp70 by covalent targeting of cysteine residues in the substrate-binding domain, J. Biol. Chem. 296 (2021).

[51] D.D. Colasurdo, M.N. Pila, D.A. Iglesias, S.L. Laurella, D.L. Ruiz, Tautomerism of uracil and related compounds: a mass spectrometry study, Eur. J. Mass Spectrom. 24 (2) (2018) 214–224.

[52] A. Capuano, G. D'Urso, M. Aliberti, D. Ruggiero, S. Terracciano, C. Festa, A. Tosco, M.G. Chini, G. Lauro, G. Bifulco, Chemoproteomics reveals USP5 (ubiquitin carboxyl-terminal hydrolase 5) as promising target of the marine polyketide gracilioether A, Mar. Drugs 22 (1) (2024) 41.

[53] A. Capuano, G. D'Urso, E. Gazzillo, G. Lauro, M.G. Chini, M.V. D'Auria, M. G. Ferraro, F. Iazzetti, C. Irace, G. Bifulco, A. Casapullo, Fatty acid synthase as interacting anticancer target of the terpenoid myrianthic acid disclosed by MS-based proteomics approaches 25 (11) (2024) 5918.

[54] S. Di Micco, V. Di Sarno, M. Rossi, V. Vestuto, T. Konno, S. Novi, M.F. Tecce, V. Napolitano, T. Ciaglia, A. Vitale, I.M. Gomez-Monterrey, G. Bifulco, A. Bertamino, C. Ostacolo, P. Blasi, A. Fasano, P. Campiglia, S. Musella, Silico identification and in vitro evaluation of new ABCG2 transporter inhibitors as potential anticancer agents 24 (1) (2023) 725.

[55] A. Shiber, T. Ravid, Chaperoning proteins for destruction: diverse roles of Hsp70 chaperones and their co-chaperones in targeting misfolded proteins to the proteasome, Biomolecules 4 (3) (2014) 704–724.